IEEE Access
Multidisciplinary | Rapid Review | Open Access Journal

Received August 23, 2016, accepted September 26, 2016, date of publication September 28, 2016, date of current version March 8, 2017.

Digital Object Identifier 10.1109/ACCESS.2016.2614329

Mobile Ad Hoc Networks in Bandwidth-Demanding Mission-Critical Applications: Practical Implementation Insights

AHMED BADER, (Senior Member, IEEE), AND MOHAMED-SLIM ALOUINI, (Fellow, IEEE)
King Abdullah University of Science and Technology, Thuwal 23955-6900, Saudi Arabia

Corresponding author: A. Bader (ahmed.bader@kaust.edu.sa)

This work was supported by the King Abdulaziz City of Science and Technology under Grant AT-34-185.

ABSTRACT There has been recently a growing trend of using live video feeds in mission-critical applications. Real-time video streaming from the front-end personnel or mobile agents is believed to substantially improve the situational awareness in mission-critical operations, such as disaster relief, law enforcement, and emergency response. Mobile ad hoc networks (MANETs) are a natural contender in such contexts. However, classical MANET routing schemes fall short in terms of scalability, bandwidth, and latency; all the three metrics being quite essential for mission-critical applications. As such, autonomous cooperative routing (ACR) has gained traction as the most viable MANET proposition. Nonetheless, ACR is also associated with a few implementation challenges. If they go unaddressed, will deem ACR practically useless. In this paper, efficient and low-complexity remedies to those issues are presented, analyzed, and validated. The validation is based on field experiments carried out using software-defined radio platforms. Compared with the classical MANET routing schemes, ACR was shown to offer up to two times better throughput, more than four times reduction in end-to-end latency, while observing a given target of transport rate normalized to energy consumption.

INDEX TERMS Mobile ad hoc networks (MANET), mission-critical applications, situational awareness, real-time video streaming, autonomous cooperative routing, path-oriented routing, geographical routing, end-to-end latency, normalized transport rate, cooperative transmission, carrier frequency offset (CFO), software-defined radio (SDR).

I. INTRODUCTION

A. MOTIVATION

Over the past few years, there has been an overwhelming growth in the use of computer vision in mission-critical applications [1]. The dissemination of live video feeds (or more generally vectors of still images) offers invaluable insights into the underlying process being monitored or controlled [2], [3]. A flagship examples entails real-time video streaming for the sake of enhancing situational awareness in mission-critical operations. Live video feed is believed to offer significant improvement in the decision-making capabilities in the wake of unexpected events [4]. In fact, the use of real-time video and vision-based data streaming for raising contextual awareness levels has been recently earning substantial interest a few other related domains such as telemedicine [5], paramedics [6], emergency & first response [7], law enforcement, and tactical operations [8].

By nature, real-time video streaming applications are typically delay-intolerant. Needless to say that video streaming (whether in raw format, thermal, or infrared) is also bandwidth-hungry. From a wireless networking perspective, it is indeed always desirable to capitalize as much as possible on the economies of scale brought forward by off-the-shelf standardized technologies. Hence, the natural technology candidates are LTE and Wi-Fi. Nonetheless, there are unfortunately some inherent deficiencies in LTE and Wi-Fi systems which render them less attractive, particularly for applications of mission-critical nature.

B. SHORTCOMINGS OF STANDARDIZED TECHNOLOGIES

LTE as a cellular technology is ubiquitous but only to a limited extent. It is straightforward to argue that there will be situations and circumstances where proper LTE service does

not exist [9]. Examples include remote onshore industrialized sites, offshore oil rigs, or deep mining pits. In fact, even in urbanized areas where coverage *does* exist, field personnel may have to be deployed in hard-to-reach areas where LTE does not penetrate deeply enough.

Another interesting example where LTE is highly likely to fall short is massively crowded events [10]. In such contexts, the sheer scale of the load that LTE networks have to withstand has an adverse effect on the bandwidth and delay performance for mission-critical applications. One may argue that mission-critical applications are typically granted preemption on the radio access network (RAN) interface by mobile operators [11]. This is a valid argument so long as the mission-critical user equipment (UE) has already managed to gain access to the network. However, gaining access to the RAN in the first place may suffer from tremendous latencies and escalated rates of failure [12]. This specifically true under high user/traffic intensities; something which is quite expected in massively crowded events. The same rationale also applies during times of natural disasters when attempts to place calls on the network throttles the network.

Unlike LTE, Wi-Fi is more of a portable technology. This is actually meant in the sense that Wi-Fi hotspots[1] can be deployed by field personnel right in the area where action is taking place. However, due to regulatory and inherent design constraints, Wi-Fi only offers a limited reach when deployed as a single-hop network.

Attempts to extend Wi-Fi service coverage span can be accomplished by means of multihop networking. However, real-world deployments have repeatedly reported some hard limits on the number of hops that Wi-Fi-based solutions can sustain [13]. This is in part due to the excessive medium access control (MAC) layer overhead plaguing Wi-Fi. As a matter of fact, the IEEE 802.11ax standard (expected to be released in 2019) is already working on means to streamline the MAC and reducing the mean time to accessing the medium [14].

Having said that, the underlying MAC layer in Wi-Fi is not fully to blame. A major contributor to the non-scalability of Wi-Fi in multihop contexts is the routing overhead. This has been coined by some researchers as a cause of ''capacity deficit'' [15] and recognized as a major challenge by the Defense Advanced Research Projects Agency (DARPA) [16]. Such a deficit or shortcoming tends to have a more profound effect as the scale (number of users and/or traffic intensity) increases as well as with increased mobility.

C. AUTONOMOUS COOPERATIVE ROUTING

As a result, there is an obvious need for infrastructure-independent ad hoc networking with strong support for mobility. Clearly, this can be articulated as a quest for a high-throughput low-latency mobile ad hoc network (MANET). Consequently, proprietary tailor-made MANET technologies are resurfacing again as viable propositions for mission-critical operations [17].

Undoubtedly, multihop MANET research literature has a mature legacy of work that is at least a couple of decades old. However, the need for significantly more bandwidth per user, ultra low end-to-end (e2e) latency, and tangibly better scalability calls for going back to the drawing board [18]. This is true since classical routing schemes are plagued by protocol overheads which have the tendency to substantially throttle the end-to-end performance of the MANET [19], [20].

To alleviate the routing overhead problem, autonomous cooperative routing (ACR) comes to rescue. In ACR, routing decisions are taking locally, i.e. wireless nodes do not revert to cross-coordination between each other before a packet is forwarded [21]. In fact, ACR does not revert to the classical concept of point-to-point (PTP) routing [18]. Rather than searching for the optimal path in a graph-based representation of the network, ACR features a seamless flow of the packet from source to destination based on a many-to-many communications paradigm [22], [23]. Any node receiving a packet will inspect its attributes based on which it decides whether to forward the packet or not. As such, the terms ''routing'' and ''relaying'' are used interchangeably throughout this paper.

D. NECESSARY IMPROVEMENTS

The MANET application scenarios considered herewith feature traffic flows which are predominantly convergecast. In other words, packets are unicast in the upstream direction to a single sink. To that end, current ACR schemes are not *fully* autonomous when it comes to unicast traffic. This is true since an end-to-end handshake must take place between each traffic source and the network sink. Such a handshake is necessary to define a ''barrage'' region (also referred to as a ''suppression'' region) between each source-sink pair. The said region serves to confine the traffic flow within certain geographical boundaries [20].

The handshake process required for spatial containment of traffic flows has to be revisited whenever significant topological changes occur, e.g. due to mobility [20]. To circumvent such a shortcoming, a novel method for constructing a fully autonomous cooperative routing (FACR) scheme is presented in this paper. The method relies on the use of a novel physical layer (PHY) frame structure coupled with geographical (position-based) routing criteria.

Recognizing the advantages of ACR/FACR in addressing mission-critical application needs, this paper unveils a few design challenges associated with these systems. The paper mainly focuses on those prime challenges which are essential for any practical and technically feasible implementation of ACR/FACR. Practical hardware and software solutions to those challenges are presented and discussed in depth. The practicality of the proposed solutions is validated on software-defined radio (SDR) platforms.

The developed hardware and software is used to carry out field tests for the sake of empirical assessment of the

[1]LTE-Unlicensed hotspots is obviously a very comparable option to Wi-Fi. In other words, it will suffer more or less from the same scalability issues outlined herewith for the case of Wi-Fi.

performance, primarily the PHY layer. The end goal is to not only to offer a public-domain insight into how ACR/FACR can be practically implemented, but also on the outstanding throughput and latency performance of this class of MANET routing.

E. PAPER ORGANIZATION

The paper is further organized as follows. Section II expands on the presentation of bandwidth-demanding mission-critical applications where computer vision is a prime element. Section III offers a brief slightly historical overview of ACR-based schemes while their advantages and virtues are detailed in Section IV. Practical implementation challenges which need to be addresses when building ACR-based systems are treated in Section V. The motivation for fully autonomous cooperative routing and means to make it happen is presented in Section VI. Finally, the experimental setup and empirical testing results are reported in Section VII then the paper is concluded in Section VIII.

II. MISSION-CRITICAL MANET APPLICATIONS

As already mentioned in Section I, the availability of live video feeds is vital in improving situational and contextual awareness in mission-critical applications. It is argued that human decision-making failures during time- and mission-critical scenarios can be caused by lack of understanding of the situation and inability to recognize the context [4]. Field commanders are consistently required to take decisions in response to unfolding circumstances. There is strong evidence that having access to live video feeds streamed from front-end personnel diminishes uncertainty and therefore enhances quality of the decision making process [7], [24].

The virtue of real-time video sharing in boosting the efficacy of mission-critical operations is quite intuitive. This is true since humans can take better decisions when offered timely and finer visibility into the underlying physical process being treated [25]. Research has also shown that the availability of real-time video communications for paramedics and first responders significantly enhances collaboration and reduces time to complete a mission [24]. As such, we've seen more emphasis on real-time video streaming for mission-critical operations in literature. For example, the U.S. National Institute of Standards and Technology (NIST) has recently released a technical note [26] in which the significance of real-time streaming for public safety operations is underlined clearly.

Real-time streaming from the field using MANET technologies can be well extrapolated to cover use cases in other industrial verticals. The prime focus of this paper is to address two general categories of mission-critical applications:

1) Defense and emergency response operations mainly encompassing tactical operations, law enforcement, fire fighting, search and rescue, crowd management, and paramedics.
2) Industrial field operations primarily in hydrocarbon exploration and production (E&P), mining, and power generation. Here, it is often required to dispatch crews of technicians and engineers to the field to execute a certain time-critical maintenance routine or react to a process failure.

In both categories, front-end field personnel are equipped with sensory that feeds back information to the back-end decision-making central. Such information is analyzed manually and/or automatically before commands and actuation instructions are fed forward to the front-end.

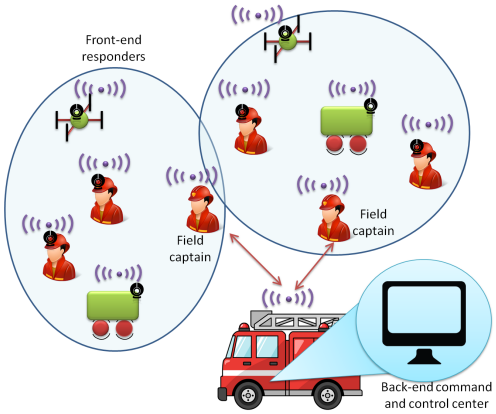

FIGURE 1. An example of public safety MANET use case. Situational awareness data (video, thermal imaging, pressure and temperature readings) flows towards the field captain and eventually to the back-end command and control central. Commands and actuation instructions are fed forward to front-end personnel as well as unmanned autonomous vehicles (UAV). Actuation instructions may include opening/closing a gate, controlling a valve, spraying of chemicals, etc.

An example of a public safety mission-critical operation is illustrated in Figure 1. From a networking viewpoint, data flow in mission-critical applications is primarily dictated by the decision-making process. Teams deployed into the field typically follow a cascaded chain of command [4], thus giving rise to inherently hierarchical team structures. Processing or even just viewing of data by front-end personnel may be an element of distraction. Thus, decision-making is by large concentrated at the back-end point. This implies that the network has to generally operate according to a convergecast rather than peer-to-peer mode.

Figure 1 also illustrates a growing trend in the vision of future mission-critical MANET. It is envisioned that unmanned autonomous vehicles (UAV) will deployed as front-end agents [27]. Within such a context, swarms of aerial or terrestrial UAVs are dispatched into the field to conduct a mission under human supervision or control. In UAV-augmented mission-critical systems, a paramount task is the joint planning and optimization of motion trajectories of the UAVs [28]. The timeliness of disseminating path planning and control signalling messages is crucial [27]. Hence, this places yet an additional level of significance for designing a low-latency MANET routing scheme.

The introduction of UAVs is also expected to hit mainstream in mission-critical industrial operations. One example is the use of UAV swarms for thermal imaging and remote sensing [29]. UAVs can be deployed in industrial facilities as a routine maintenance measure, or as part of a emergency response mission. It is also worthwhile to mention at this point that UAV swarms have been also considered for 3D mapping, surveying, and other civil engineering tasks [30]. The value proposition of deploying UAVs alongside human agents is manifested in the reduction of time to complete a mission, reduce injury rates, achieve better field coverage, and improving accessibility into hard-to-reach spots.

III. AUTONOMOUS COOPERATIVE ROUTING BACKGROUND

The goal of this subsection is not to offer a detailed literature survey of ACR-driven routing schemes. Rather, it aims at offering a brief historical background and some insight into the motivations for ACR. In the next subsections, some of the most prominent incentives for adopting ACR schemes are presented in more depth.

Indeed, MANET is a well-established research field that is at least a couple of decades old. Point-to-point (PTP) routing paradigms (also referred to as path-oriented schemes [31]) have dominated the scene for quite some time [18]. As the foremost contender in this realm, geographical routing (geo-routing) has been widely adopted in the context of MANET. This is primarily due to its resilience to mobility and network topological changes [32]. As a matter of fact, geo-routing has been embraced by the European Telecommunications Standards Institute (ETSI) as a standard MANET routing scheme for Intelligent Transport Systems (ITS) [33].

However, current implementations of geo-routing are unfortunately plagued by an overhead that grows rapidly with node density and/or frame arrival rate [21]. This indeed has adverse consequences on latency and throughput performance. Such an issue has already been identified and prioritized as a serious challenge for MANETs [15], [16].

Broadly speaking, classical geo-routing may take one of two forms. The first is beacon-based whereby position beacons are exchanged among neighboring nodes, so as to maintain up-to-date topological awareness. In contrast, beaconless geo-routing entails receiver-based contention to select the best packet forwarder [23]. Both forms however suffer from the aforementioned problem: they tend to incur large overheads either due to the exchange of neighbor discovery messages (beacon-based protocols), or due to contention resolution overhead (the beaconless case) [34].

The routing protocol overhead ought to be diminished in order to meet the aspirations set forth for mission-critical applications. As such, cooperative transmission comes to rescue. From a conceptual point of view, autonomous cooperative relaying was formally introduced for the first time by [35] and [36]. The relaying mechanism was actually dubbed there as ''randomized distributed cooperative transmission''. Autonomous cooperative transmission was analyzed from the perspective of achievable cooperative transmit diversity in great depth in [37] and [38].

In essence, autonomous cooperative relaying entails the forwarding of physical frames while not reverting to any relay selection process. The term *autonomous* mainly stems from the fact that nodes within a cooperative cluster are actually unaware of each other [18]. In other words, there does not exist any sort of cross-coordination between nodes before the frame is relayed. Therefore, autonomous cooperative routing is also often referred to as ''blind cooperative transmission'' [39].

The transformation of ACR concepts into practice entailed the need to find means for confining the packet flows spatially. Otherwise, unicast flows will quickly flood the network and unnecessarily hijack the spatial and temporal resources of the network [23]. As such, controlled barrage or suppression regions must be created by means of request-to-send (RTS)/clear-to-send (CTS) handshake between any arbitrary pair of source-sink nodes [18]. Traffic from a source to a given sink is suppressed and barred to spill outside the designated barrage region [22]. This line of work has been holistically treated in a series of papers in [8], [17], [18], [20], [40], and [41]. To guarantee positive progress towards the sink, hop-count to reach the sink is adopted as a routing metric.

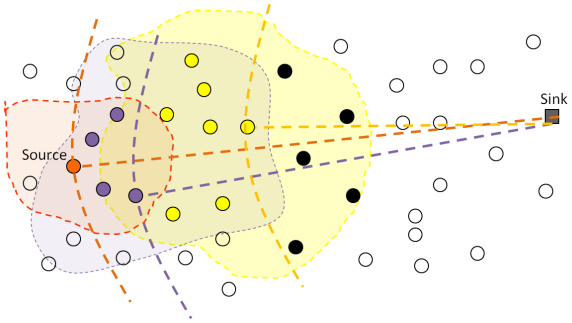

FIGURE 2. Illustration of the operation of an autonomous cooperative scheme. A source injects a frame into the network. Receivers who are closer to the sink than the source will relay the frame. In the second hop, each receiver reads the position information conveyed by the transmitters of the first hop in order to decide whether to forward the frame or not. Any second-hop receiver offering positive progress towards the sink will forward it. The forwarding process continues seamlessly until the frame reaches its destination.

In case position information is available to nodes, then position-based routing criteria can be used to streamline the forwarding process within narrow geographical corridors [21]. One possible manifestation of such approach is illustrated in Figure 2. As shown in the figure, only nodes offering positive progress towards the sink take on the responsibility of forwarding the packet. Once a node receives a packet, it inspects the position attributes of the transmitters and compares them to its own. The PHY header has to be designed in a way that supports such a functionality as further described in Section VI-B. A simple geo-routing criterion is to for the receiver to forward the packet if it is closer than at least a certain number of transmitters.

TABLE 1. List of notations.

T_p	data packet duration	T_t	time to transition between Tx and Rx states
T_c	control packet duration	T_w	waiting time before successful channel access
T_b	fixed back-off timer	T_{h_q}	duration of the qth hop
Q	average number of hops to destination	d	hop distance (positive progress towards destination)
T_R	PHY header duration	P_t	transmit power
P_n	noise power	τ	threshold on outage probability
γ_t	SINR threshold for successfully decoding a frame	α	large-scale path-loss coefficient
γ_o	mean SINR	a	hop distance gain of ACR over PTP
I	number of cooperative transmitters	N	number of nodes in the network
$p(N)$	probability that a node is a destination	$A(N)$	area of the communications footprint
R_{max}	maximum achievable per-node throughput	W	over-the-air bit rate
P_b	back-off probability	D	source-destination separation
l_A	packet arrival rate	l_e	effective packet arrival rate
λ	wavelength		in case of path-oriented routing
ρ	node density	$\overline{M}$	average number of nodes backing off
Δ_f	subcarrier bandwidth	N_s	FFT size, number of samples per OFDM symbol
$T_s = \frac{1}{N_s \Delta_f}$	sampling time	$t = nT_s$	discrete time representation
$k = -\frac{N}{2} \dots \frac{N}{2}$	subcarrier index	$i = 1 \dots I$	multi-node transmitters
δ_i	CFO of ith multi-node transmitter with respect to Rx	$a_{k,n} e^{j\phi_{k,n}}$	QAM symbol time n and subcarrier k
$h_{i,m}, m = 1 \dots \mathcal{M}$	channel fading coefficients	T	time between multipath channel components
$T_i^{'}$	propagation delay plus cooperative time offset associated with transmitter i	T_s	signal sampling interval
		x_i^n	phase rotation of the ith cooperative transmitter
$N^{'}$	effective number of nodes (barrage region update)	T_U	total duration to update barrage regions
S_R	number of times barrage update is repeated	$\mathcal{C}(\mathcal{UV})$	number of hops measured from node $\mathcal{U}$ to V
B_L	number of localization resource blocks	B_q	number of relative position quantization tones
p_{st}	probability of successful triangulation	F	number of trials before successful triangulation
L	number of bits in a data packet	P_o	outage probability

The concurrent transmission of the same PHY frame provides for an array gain that is proportional to the number of transmitters at a given hop [22]. Such a gain contributes to the increase in the average hop distance and consequently reduces the e2e latency. Nonetheless, it also means substantially higher energy consumption per frame at a single hop. This important tradeoff is analyzed and treated rigorously from an e2e perspective in [21]. It is shown there that for a given e2e energy consumption target, ACR can be tweaked to offer tangibly lower e2e latency.

IV. WHY AUTONOMOUS COOPERATIVE ROUTING?

In this section, the advantages of ACR in comparison to path-oriented (i.e. PTP-based) routing schemes are studied. Three prime metrics are considered herewith: end-to-end latency, normalized transport rate, and maximum achievable throughput. A list of all notations used in the paper is given in Table 1.

A. LOWER END-TO-END LATENCY

The end-to-end latency is given by $\sum_{q=1}^{Q} T_{h_q}$. Here, Q denotes the expected number of hops from source to sink assuming that a barrage (i.e. suppression) region has already been allocated for a given traffic flow. Further, T_{h_q} is the duration of the qth hop. In the case of ACR, the hop duration T_{h_q} is deterministic since there is no contention amongst potential relays. Accordingly, $T_{h_q} = T_p + T_t$, where T_p is the packet duration and T_t is the turn-around time corresponding to the change from receiver state to transmitter state.

On the other hand, path-oriented routing schemes entail some overhead pertaining to the selection of the optimal path. In the sequel, classical beaconless geo-routing is considered as a representative example. The sender needs to select the best relay, typically the one offering largest positive progress towards the destination. The selection is established through a handshake process. At the bare minimum, such a process consists of three transactions at *each* hop [34]:

1) Request-to-send (RTS) message of duration T_c followed by a turnaround time T_t.
2) A clear-to-send (CTS) message from the optimal receiver with duration that is also equal to T_c followed by T_t.
3) Packet transmission with duration T_p.

The hop duration is therefore $T_{h_q} \geq T_p + 2T_t + 2T_c$ which is obviously always greater than that of the autonomous case. Therefore, end-to-end latency as a performance metric speaks in favor of ACR.

There is another factor that further boosts the latency performance of ACR. That is related to the fact that ACR exploits cooperative transmission techniques which in return feature array (power) gains [22]. Moreover, with some precoding and transmit-side signal processing, transmit diversity gains can be also attained [37]. By means of applying carefully selected randomization matrices to the transmitter vectors, such diversity gains can be obtained. To some extent, this approach has similar effect to the so-called phase dithering [42].

The array and diversity gains result in extending the average communication range compared to path-oriented routing. Undoubtedly, this results in reducing the number of hops Q, thus further contributing to the reduction of the end-to-end latency. This is true since $\sum_{q=1}^{Q} T_{h_q}$ is a decreasing monotone

in Q. A rigorous analysis of the progress made per hop in ACR networks can be found in [21].

B. HIGHER NORMALIZED PER-HOP TRANSPORT RATE

The normalized transport rate (NTR) is defined as the average number of bits that can be communicated at a given hop over distance per unit time using one unit of energy [43]. The consideration of the normalized transport rate as a performance metrics stems from its ability to capture hop distance (which eventually affects end-to-end delay) as well as energy consumption.

Recalling that a contention phase ought to take place before a packet is routed in path-oriented schemes, then the upper bound on NTR is dictated by two factors:

1) The minimum duration of a contention phase.
2) The maximum achievable hop distance.

The hop distance has many definitions in literature, but here it is assumed that it refers to the positive progress made at a given hop along the line connecting the source to the destination. In the case of path-oriented schemes, assuming the mean hop distance to be equal over all hops is an acceptable approximation (especially in dense scenarios) [31], [44].

The hop distance, denoted by d, is governed by the underlying outage model. In a Rayleigh fading channel, the mean signal to noise and interference ratio (SINR) is given by:

$$\gamma_o = \frac{2P_t}{P_n}\left(\frac{\lambda}{4\pi d}\right)^{\alpha}, \tag{1}$$

where λ is the wavelength, α is the large-scale path loss coefficient, P_t is the transmit power, and P_n is the noise power. The outage probability is given by $\mathrm{P}_o = 1 - e^{-\gamma_t/\gamma_o}$, where γ_t is the below which the receiver will be in outage. Consequently, the hop distance given a single transmitter d is expressed as:

$$d \leq \left(\frac{\lambda}{4\pi}\right)\sqrt[\alpha]{\frac{2P_t \ln\frac{1}{1-\tau}}{P_n\gamma_t}}. \tag{2}$$

On the other hand, the duration of one complete contention phase cannot be shorter than one RTS message from the sender, one CTS message from the relay, plus the packet duration, T_p. As mentioned earlier, the half-duplex nature of the devices entails a turn-around time of T_t. Accordingly, the NTR for PTP-based routing is upper bounded by:

$$NTR_{PTP} = \frac{Ld}{\left[2(T_c + T_t) + T_p\right]P_t(T_p + 2T_c)}, \tag{3}$$

where L is the length of a packet in bits. On the flip side of the coin, the NTR for the autonomous case is given by:

$$NTR_{ACR} = \frac{Lda}{(T_p + T_R)^2 IP_t}, \tag{4}$$

where I is the number of cooperative transmitters, T_R is the duration of the PHY header, and a is a gain factor which reflects the fact that the hop distance in cooperative transmission mode is generally larger than PTP mode. There are indeed many factors affecting the value of a. Nonetheless, for the sake of simplification and conciseness of the analysis, the special case of I equidistant transmitters can be considered here. In such a case, $a = I^{1/\alpha}$. Accordingly, it can be shown from (3) and (4) that ACR-based systems offer better NTR under the condition that:

$$I^{1-\frac{1}{\alpha}} < \frac{[2(T_c + T_t) + T_p](T_p + 2T_c)}{(T_p + T_R)^2}. \tag{5}$$

The values of T_p, T_c, T_t and T_R are mainly dictated by the underlying video transmission quality of service (QoS) requirements as well as hardware constraints.

In Section VII, a proprietary PHY implementation developed for this project is described in more detail. The implemented PHY is based on the use of orthogonal frequency division multiplexing (OFDM). The duration of one OFDM symbol is set at 8 μs. The duration of the PHY header is equal to 1 OFDM symbol. The preamble training sequence has the duration of exactly 38.4 μs. Therefore, the shortest frame (i.e. one that is sufficiently large to carry an RTS or CTS control message) is $T_c = 54.4\mu$s. The turn-around time, T_t, is highly dependent upon the underlying radio front-end. In this specific implementation it was measured to be around 180 μs.[2] Finally, the payload portion was set to consist of 50 symbols. While lower frames may be preferable from a frame error rate (FER) viewpoint, they are associated with larger PHY overhead ratio. A frame of 50 symbols i.e. $T_p = 476.8\mu$s, strikes the right balance.

Based on the above, and assuming a path loss coefficient of $\alpha = 3$, then ACR outperforms PTP-based path-oriented scheme for $I < 3.02$. In other words, autonomous geo-routing offers higher NTR as long as is carried out by one, two, or three transmitters at a given hop.

C. HIGHER MAXIMUM ACHIEVABLE THROUGHPUT

The end-to-end latency performance is indicative but not sufficient to establish with evidence the superiority of ACR. Interference caused by other concurrent packet flows indeed has an adverse effect on e2e latency since it causes transmission outages and invokes back-off procedures. Hence, it must be taken into consideration. The interplay between interference and medium access is best captured by studying the maximum achievable throughput per node.

It was shown in [31] that ACR-based networks offer a per-node unicast capacity which scales in the order of $\Theta(\sqrt{N/\log N})$. This is identical to the Gupta-Kumar per-user capacity [45] that traditional path-oriented routing networks can offer. While such a result is reassuring, asymptotic scaling orders do not suffice to benchmark ACR against path-oriented PTP-based routing schemes. Furthermore, video streaming traffic in a mission-critical MANET is predominantly convergecast. As such, this must be taken into consideration.

Bisnik and Abouzeid provided a detailed throughput and delay analysis in a random access multihop

[2] A video capture of the turn-around time measurement is posted online for the interested reader (https://youtu.be/lDYVHZ6GcIM.).

network [46] and [47]. For a network of N nodes, an absorption probability $p(N)$ is defined therewith as the probability that a traffic flow is terminated at an arbitrarily chosen node. It is straightforward to state that $p(N) = 1/N$ in a convergecast network.

Assuming a persistent back-off scheme [48], the mean waiting time before successful channel access is denoted by T_w. The backoff footprint, $A(N)$ is defined as the area around a given transmitter within which no other transmission can take place due to interference. $A(N)$ is actually normalized by the total area of the network. Finally, the maximum achievable throughput per node, R_{max}, is defined to be the maximum node throughput for which the end-to-end delay remains finite. Subsequently, R_{max} (in bps) is computed using [46], eq. (22):

$$R_{max}(N) = \frac{Lp(N)}{T_w + \frac{L}{W} + 4NA(N)\frac{L}{W}}, = \frac{L}{NT_w + NT_h + 4N^2A(N)T_h}. \quad (6)$$

where W is the bit rate.

The mean waiting time T_w is function of the back-off probability. The latter can be expressed as $P_b = \overline{M}/N$, where $\overline{M}$ is the average number of nodes who are forced to queue at least one frame of their own during the entire multihop journey of another frame [49]. Assuming Bernoulli distribution, the mean number of transmission attempts before success is $1/P_b$. As such, the mean back-off time can then be expressed as:

$$T_w = (1 - P_b)T_b = \left(\frac{N}{N - \overline{M}}\right) T_b, \quad (7)$$

where $T_b \geq T_h$ is a fixed duration a node must wait before reattempting to retransmit.

To compute $\overline{M}$, first the probability that exactly m nodes will back off during a given hop is analyzed. Given n nodes exist in the back-off region and a packet arrival rate of l_A, then this probability is given by:

$$p_m(m|n) = \binom{n}{m} \left(1 - e^{-T_h l_A}\right)^m \left(e^{-T_h l_A}\right)^{n-m}, m \leq n. \quad (8)$$

The probability that exactly n nodes actually exist in the region is:

$$p_n(n) = \frac{1}{n!}(\rho A)^n e^{-\rho A}, \quad (9)$$

where ρ is the network node density under the assumption of 2D Poisson point process node distribution. Consequently, the probability distribution function of m is given by:

$$p_m(m) = \sum_{n=m}^{\infty} p_m(m|n)p_n(n). \quad (10)$$

The next question to tackle: in light of the above, what is the probability, $P_M(M)$, that M sensor nodes backlog at least one transmission during the Q-hop lifetime of the packet in concern? The different permutations for distributing those M nodes over Q hops can be conveniently computed using integer set partitioning algorithms. These permutations can be expressed in matrix format as

$$\begin{bmatrix} m(1,1) & \dots & m(1,Q) \\ \vdots & \ddots & \vdots \\ m(\mathcal{P},1) & \dots & m(\mathcal{P},Q) \end{bmatrix} \in \mathbb{Z}^{\mathcal{P}\times Q}, \quad (11)$$

where $\mathcal{P}$ equals the number of different permutations corresponding to the distribution of M back-off nodes over Q hops. Consequently, the probability density function is obtained as follows:

$$P_M(M) = \sum_{u=1}^{\mathcal{P}} \prod_{i=1}^{Q} p_m(m(u,i)). \quad (12)$$

Therefore, a compact expression for $\overline{M}$ can be obtained as follows:

$$\overline{M} = \sum_{M=0}^{\infty} \sum_{u=1}^{\mathcal{P}} \prod_{q=1}^{Q} \sum_{n=m(u,q)}^{\infty} Mp_m(m|n)p_n(n). \quad (13)$$

Substituting (13) into (7) gives the mean waiting time before successful channel access, T_w. It is paramount however to note that listen-before-talk (and consequently back-off procedures) is applied only once at the source in case of autonomous routing. On the other hand, it is applied at *each* intermediate hop in case of PTP-based (i.e. path-oriented) routing. In other words, the back-off procedures are invoked every time a node has a packet to send whether its own or an ingress packet from a neighboring node. Hence, the effective packet arrival rate in case of path-oriented routing is actually:

$$l_e = \frac{l_A}{p(N)} = Nl_A. \quad (14)$$

The computation of T_w and subsequently R_{max} is highly dependent on the mean number of hops, Q, as can be inferred from the analysis above. For a source-destination separation of D, the average number of hops in PTP-based systems is more or less $Q = \lceil D\sqrt{\frac{\pi}{A(N)}} \rceil$. On the other hand, such an approximation does not hold true in ACR-based systems. This is because in the long-term average sense, the hop distance grows in size every hop [21], [22]. As such, it is mandatory to derive a means to compute the probability mass function (PMF) of Q, which is the task to tackle next.

The probability of hopping Q times before reaching the destination is expressed as $p_Q(Q) = \mathbb{P}[x_Q \geq D]$, where x_Q is the total progress made after Q hops along the axis connecting the source and the destination. The number of cooperative transmitters at hop i is denoted by I_i. Further, the cumulative number of cooperative transmitters from the first hop till the $(Q-1)$th hop is given by $S_{Q-1} = \sum_{i=1}^{Q-1} I_i$.

An expression for the total progress made by the packet after Q hops was derived in [21, eq. (9)] and is recalled here for convenience:

$$x_Q = \varphi S_{Q-1} + (Q-1)\frac{\beta}{U^{\frac{1}{\alpha}}} + x_1. \quad (15)$$

In (15), φ and β are network-dependent parameters, α is the large-scale path loss exponent, x_1 is the progress made in the first hop, and U is and outage-dependent constant that is given by [21]:

$$U = \frac{P_n}{2P_t}\left(\frac{4\pi}{\lambda}\right)^{\alpha}\frac{\gamma_t}{\ln\frac{1}{1-\tau}}. \quad (16)$$

It was also demonstrated in [21] that the PMF of S_{Q-1} can be computed for a given set of network parameters by recursion. Therefore, the PMF $p_Q(Q)$ can be computed numerically using:

$$p_Q(Q) = \mathbb{P}\left[S_{Q-1} \geq \frac{1}{\varphi}\left(D - \frac{\beta}{U^{1/\alpha}}(Q-1) - x_1\right)\right]. \quad (17)$$

With the PMF readily available, the mean value of Q can be then easily computed.

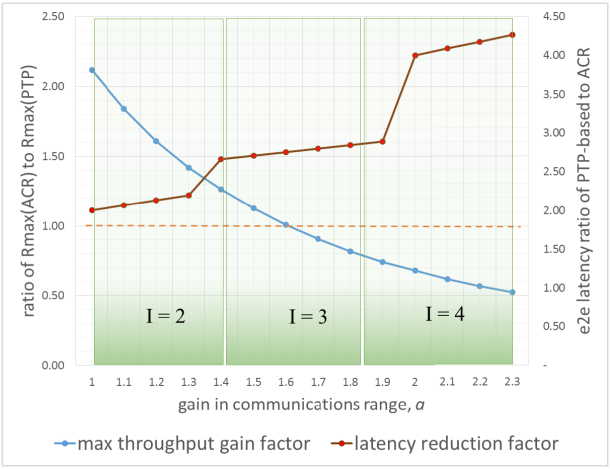

FIGURE 3. The performance of ACR is compared to PTP-based routing in terms of maximum achievable per-node throughput as well as end-to-end latency. Using the analytical results of Section IV, the computations were carried out assuming a network of 20 nodes at a density of $\rho = \frac{1}{30^2}\,\mathrm{m}^{-2}$. The average PTP communication range was $\leq$ 20m at a path loss coefficient of 2.8. Packet duration of 0.5 ms is assumed at an arrival rate of $100\mathrm{s}^{-1}$.

The ratio of R_{max} for ACR to that of PTP-based was computed using (6) - (17). Results are shown in Figure 3 in terms of the communication range gain, a. For a better and more insightful perspective, the e2e latency reduction factor that ACR enjoys over PTP-based routing is also plotted on the same figure. The plot in Figure 3 is divided into 3 segments corresponding to the number of cooperative transmitters covering a given range of gain. Empirical results obtained from field testing and reported in Section V have been used to deduce the value of I corresponding to a range of values for a.

Although a larger value of a favors ACR in terms of end-to-end latency, it is not always preferable in terms of throughput performance. It is evident from the figure that ACR starts to lose its edge in terms of per-node throughput as a increases. This is mainly because the coverage footprint of a packet transmission grows, thus blocking other nodes from accessing the network [31]. As such, it is essential to tune down the individual transmit power so that a is maintained within limits.

D. SUMMARY

It is worthwhile at this point to summarize the key findings so far. To compare ACR to classical path-oriented routing schemes, it is best to fix the NTR as a performance constraint since it is the one that captures energy consumption. It has been already shown that with $I = 3$, ACR and path-oriented schemes offer the same NTR. However, it is clear from Figure 3 that ACR offers up to 2X improvement in the maximum achievable throughput per node. It can be also inferred that ACR enjoys at least 4X reduction in the end-to-end latency. A corollary to this statement is that if throughput and latency targets are fixed, ACR will consume substantially less energy per transported bit. Looking at it from either perspective, ACR outperforms classical PTP-based path-orient MANET routing by far.

A final note should be tailored for security aspects. Indeed, security is a paramount concern in mission-critical applications and should not be overlooked. However, it is quite an involved task to benchmark the performance of ACR protocols to path-oriented ones in terms of susceptibility to malicious attacks. Recognizing its importance, analysis of security aspects for ACR is left as future scope of work.

V. PRACTICAL IMPLEMENTATION CHALLENGES

The goal of the previous section was to establish with evidence the superiority of ACR in bandwidth-demanding mission-critical applications. Next, attention shall be geared towards some of the practical implementation challenges. Such challenges mainly stem from the non-traditional wireless channel characteristics in a cooperative transmission setup. As such, this section starts off with the presentation of the channel model and then immediately delves into PHY design challenges invoked by the cooperative channel. Remedies and solutions are highlighted as well.

A. WIRELESS CHANNEL MODEL

From a PHY perspective, ACR in essence is a technique that allows multiple nodes to transmit the same frame concurrently. This statement needs to be qualified at two different time scales. Concurrency is really true only at the packet, i.e. medium access control (MAC) layer level. At the symbol-level however, the cooperative transmitters are not perfectly aligned in time. In other words, the channel model has to accommodate the case of asynchronous transmission case.

In most recent literature, the case of asynchronous cooperative transmission has been referred to as the cooperative time offset (CTO) [50]. Even in the case of perfect synchronization amongst the I cooperative transmitters (e.g. by means of having access to GPS), there will still be time offsets from the receiver perspective due to propagation delay differences. Both effects are captured in the cooperative channel model by introducing the delays $T_1' \ldots T_I'$ as illustrated in Figure 4.

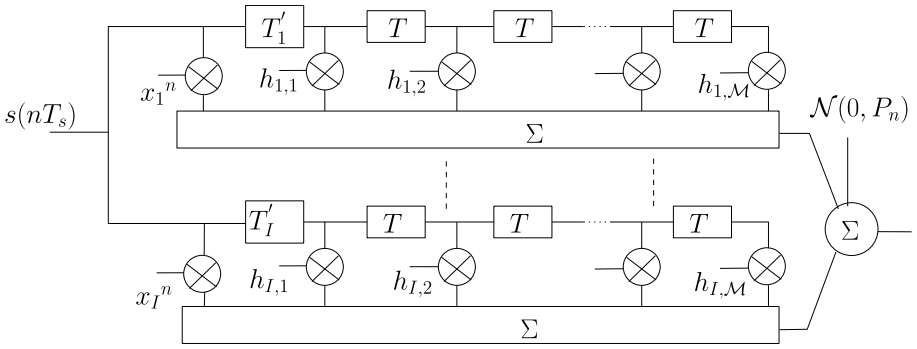

FIGURE 4. Composite channel response capturing CFO plus doppler spread, propagation delay differences, as well as multi-path channel effects.

The channel between an arbitrary pair of nodes is represented by a generic wideband frequency-selective multipath tap-delay line with Rayleigh-distributed tap gains [51]. On average, there are $\mathcal{M}$ such taps. Natural echoes due to multipath are grouped in intervals of duration of T seconds. Mobility speeds are with the pedestrian to slow vehicular ranges such that the fading coefficients are assumed to be quasi-static, i.e. they remain constant during a single frame.

Orthogonal frequency division multiplexing (OFDM) is employed as a measure to counteract that frequency selectivity of the cooperative channel. The duration of the OFDM symbol is assumed to be larger than $(\mathcal{M}-1)T+\max\{T_i^{'}\}_{i=1}^{I}-\min\{T_i^{'}\}_{i=1}^{I}$ ensuring that each subcarrier encounters approximately a frequency-flat fading [52]. Amending each OFDM symbol with a cyclic prefix eliminates inter-carrier interference (ICI) and restores orthogonality between subcarriers. This enables decoupled signal detection at each subcarrier.

Under the reasonable assumption that the fading coefficients $h_{i,m}$ are all mutually independent, it follows that $H(f)$ is complex Gaussian such that $H(f) \sim \mathcal{N}(0, \sigma_S^2)$, with

$$\sigma_S^2 = \sum_{i=1}^{I}\sum_{m=1}^{\mathcal{M}} \mathbb{E}[|h_{i,m}|^2]. \tag{18}$$

Furthermore, $|H(f)|^2$ is exponentially distributed with a mean of $2\sigma_S^2$. We note that $\sum_{m=1}^{\mathcal{M}} \mathbb{E}[|h_{i,m}|^2]$ represents the mean power content of the channel between the receiver and the ith transmitter and is equal to $(\lambda/4\pi d)^{\alpha}$. Therefore, we obtain:

$$\sigma_S^2 = \left(\frac{\lambda}{4\pi}\right)^{\alpha} \sum_{i=1}^{I} \frac{1}{d_i^{\alpha}}. \tag{19}$$

It is assumed that the duration of the cyclic prefix of the OFDM symbol is long enough such that all signal echoes (natural and artificial) arrive within the cyclic prefix interval. Other ongoing packet relaying processes will rather contribute to the interference signal. This interference however will be also Gaussian since the individual channel gains are Gaussian [53]. The exact nature of such an external interference is beyond the scope of the present work.

B. COOPERATIVE CARRIER FREQUENCY OFFSET

The sampling frequency is $1/T_s$, and n is a running sample index. The number of subcarriers is denoted by N_s. Due to clock imperfections, a carrier frequency offset (CFO) naturally exists between any arbitrary pair of nodes. The CFO between transmitter i and the receiver is denoted by $\delta_i^{(CFO)}$. The cooperative carrier frequency offset (CCFO) is defined herewith as $\max_i \delta_i^{(CFO)} - \min_i \delta_i^{(CFO)}$. On the other hand, all nodes are assumed to be mobile, thus a frequency doppler exists between the ith transmitter and the receiver and is denoted by $\delta_i^{(DOP)}$. The CFO and the doppler shift together have the combined effect of causing a phase rotation. Such an effect is captured in the model of Figure 4 by defining:

$$x_i \triangleq e^{j2\pi\delta_i \frac{1}{N\Delta f}} \ , \ \delta_i = \delta_i^{(CFO)} + \delta_i^{(DOP)}. \tag{20}$$

Hence, taking the individual CFO and doppler shift effects into consideration, the baseband signal transmitted by node i is expressed as:

$$\begin{aligned} s_i(nT_s) &= \sum_{k=-\frac{N_s}{2}}^{\frac{N_s}{2}} a_{k,n} e^{j\phi_{k,n}} e^{j2\pi(k\Delta f+\delta_i)nT_s} \\ &= x_i^n \sum_{k=-\frac{N_s}{2}}^{\frac{N_s}{2}} a_{k,n} e^{j\phi_{k,n}} e^{j2\pi kn/N_s}, \end{aligned} \tag{21}$$

where $a_{k,n}e^{j\phi_{k,n}}$ is the transmitted symbol. Consequently, the frequency-domain response of the composite channel is given by:

$$H(n,f) = \sum_{i=1}^{I} x_i{}^n e^{-j2\pi f T_i^{'}} \sum_{m=1}^{\mathcal{M}} h_{i,m} e^{-j2\pi f(m-1)T}. \tag{22}$$

From (22), it is clear that the channel is highly time-varying because of the CCFO. This is true even though the fading coefficients are assumed to be quasi-static.

The time-varying nature of the channel mandates robust receiver design. As a matter of fact, the detrimental effect of the CCFO is far more adverse than that of the doppler spread alone. This is true since the CCFO can be orders of

magnitude larger. This is better appreciated by means of an example. A 1-ppm free-running clock yields a CFO around ±2400 Hz at a center frequency of 2.4 GHz. In comparison, the maximum doppler shift for a node moving at 10 km/hr for example is less than 25 Hz. Consequently, it is evident that the CCFO problem is order of magnitude more challenging than the classical doppler spread problem.

In the presence of CCFO, the channel coherence time (roughly equal to the 0.423 times the reciprocal of the maximum doppler shift [51]) in case of free-running clocks is comparable to the duration of just few OFDM symbols. The CCFO poses a couple of serious challenges on receiver design which has to cater for such a highly dynamic and fast-changing conditions. Two of such challenges along with viable remedies are outlined in the following.

1) AUTOMATIC GAIN CONTROL AGING

The purpose of automatic gain control (AGC) in the receiver is to perform pre-amplifier gain adjustments. These adjustments are required in order for the signal to be received within the dynamic range of the analog-to-digital converter (ADC) [54]. The AGC module typically operates on the preamble portion in the very beginning of the PHY frame. It is in essence a feedback control loop whose goal is to maximize the input signal within the linear range of the ADC.

The correlation coefficient between two time samples of the Rayleigh fading envelope separated by τ_v is given by the zeroth-order first kind Bessel function $J_o(2\pi\delta_i\tau_v)$ [51]. For illustration purposes, the correlation coefficient for the case of zero CCFO (i.e. in the presence of only doppler shifts) is compared to a 500-Hz CCFO on the same time scale in Figure 5.

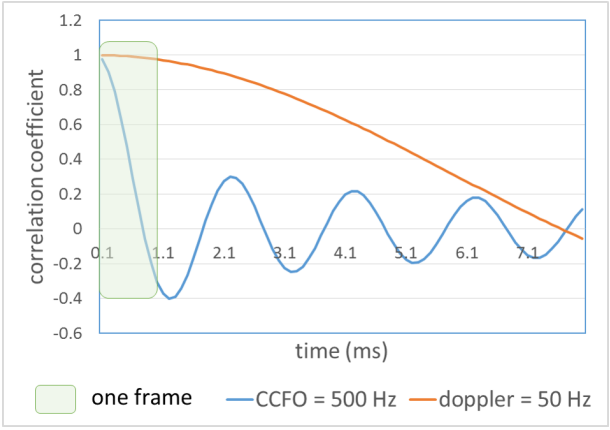

FIGURE 5. Correlation coefficient of the fading channel envelope in case of zero and 500-Hz CCFO. In both cases, the doppler shift is assumed to be 50 Hz. It is evident that CCFO produces a highly time-varying channel and consequently the channel gains quickly become uncorrelated even within the time scale of a single PHY frame.

From Figure 5, it is apparent that the AGC gain value will quickly become outdated in the presence of CCFO. This is also referred to as AGC aging. By the end of the frame, the outdated AGC value will be either:

1) Too high, therefore driving the incoming signal to the non-linear range of the ADC and causing significant signal distortion.
2) Unnecessarily too low, thus the received signal may suffer from a severe SNR drop.

To address the AGC aging problem, there is the obvious option of using shorter PHY frame durations. Nevertheless, this will indeed increase the PHY overhead ratio and hence adversely affect the throughput. A more preferable option is to rerun the AGC module on pilots tones which are inserted within the PHY frame. The AGC loop may take quite a few samples in the beginning of the frame to converge. This is true since the channel variation from frame to frame may be unpredictably high. A new frame is a new transmission with a new set of cooperative transmitters. Hence, the power of the incoming signal is uncorrelated to that of the previous frame. On the other hand, the convergence time of the AGC loop when run on pilots is much faster. This is true since the channel variation within a frame is statistically correlated.

2) AGING OF CHANNEL ESTIMATES

Similar to the AGC, channel estimation is typically performed on the preamble portion as well. Specifically, the preamble includes a long training sequence (LTS) symbol that is known a priori to the receiver. In OFDM systems, the LTS is used to estimate the fading channel coefficients corresponding to each frequency subcarrier [50]. Due to the highly time-varying nature of the channel, the estimates of the fading coefficients obtained in the beginning of the frame quickly become obsolete. In the presence of CCFO, the coherence time of the channel can be much shorter than the frame duration. As such, channel estimates need to be updated more often.

One approach is to insert more training symbols (i.e. LTS symbols) within the payload portion of the PHY frame. However, this will significantly increase the PHY overhead. This is true particularly since the coherence time is too small. For example, if the CCFO is 1000 Hz, then the coherence time of the channel is about 425 μs. A good design practice is to ensure up-to-date channel coefficients at least at a rate of 10 times per coherence window, i.e. an LTS symbol must be inserted once every 42.5 μs. For a symbol duration of 8 μs, this means that an LTS must be inserted at least after every 5th symbol. Hence, the overhead contribution of channel estimation is in excess of 16% which is quite significant.

In an attempt to relax such an overhead, one may argue for farther spacing LTS symbols in the time domain. Such a proposition would entail the use of linear interpolation to compute the amplitude and phase of the channel coefficients for OFDM symbols in between the LTS symbols. However, as Figure 6 strongly suggests, the level crossing nature of the cooperative channel is quite aggressive thus rendering the linear interpolation option very risky.

A neater approach on the other hand is to autonomously estimate the channel in a continuous fashion using the well-known decision-directed estimation (DDE) method [55].

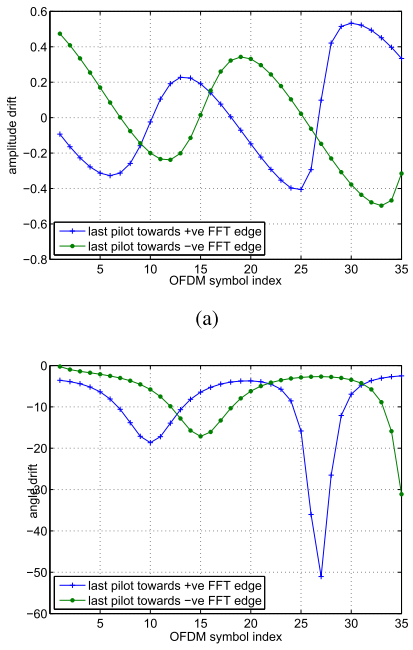

FIGURE 6. Cooperative transmission in the presence of CCFO induces significant fluctuations in the phase and amplitude of channel fading coefficients. Thus, linear interpolation is by large infeasible. (a) Amplitude drift over time. (b) Phase drift over time.

Each OFDM symbol consists of N_s samples. At the end of the LTS (which is the first symbol in the frame), the least squares (LS) channel estimate at subcarrier k is given by:

$$\widehat{H}(1,k) = \frac{\sum_{n=1}^{N_s} s^*(N_s-n,k)r(N_s-n,k)}{\sum_{n=1}^{N_s} |s(N_s-n,k)|^2}, \qquad (23)$$

where $r(n,k)$ is the received signal observed at the nth time sample at the kth subcarrier of the fast Fourier transform (FFT) stage output. In (23), $s(n,k) = p(n,k)$ when k is pilot tone, otherwise $s(n,k) = \hat{s}(n,k)$, i.e. the decided symbol. To obtain the channel estimate at any other arbitrary symbol $z = 2, 3, \ldots$, recursive estimation can used as follows:

$$\hat{H}(z,k) = \frac{\hat{y}(zN_s,k)}{\hat{Y}(zN_s,k)}, \qquad (24)$$

where

$$\hat{y}(z+1,k) = \hat{y}(z,k) + r(z,k)s^*(z,k) - r(z-1,k)s^*(z-1,k) \qquad (25)$$

$$\hat{Y}(z+1,k) = \hat{Y}(z,k) + |s(z,k)|^2 - |s(z-1,k)|^2. \qquad (26)$$

A DDE receiver was incorporated into the PHY implementation which is further discussed in Section VII. Empirical results reported therewith offer clear evidence that using DDE is quite viable in treating the channel estimate aging effect.

Finally, it is worthwhile to mention that the consistent availability of a global positioning system (GPS) signal would indeed help synchronize cooperative transmitters and thus eliminate the CCFO problem. However, it is important also to emphasize that losing the GPS signal for just a few seconds may cause transmitters' clocks to drift substantially and therefore the CCFO problem reemerges again. This is why it is paramount to fortify receivers with GPS-independent algorithms.

C. COOPERATIVE POWER DELAY PROFILE

The power delay profile (PDP) of the cooperative channel is unique in the sense that it contains many strong yet slightly delayed signal arrivals. This creates a power spectral density (PSD) shape that is also fundamentally different from that corresponding to the classical PTP channel. This is illustrated in Figure 7. As a consequence, the PDP of the cooperative channel brings forward two PHY design challenges as explained in what follows.

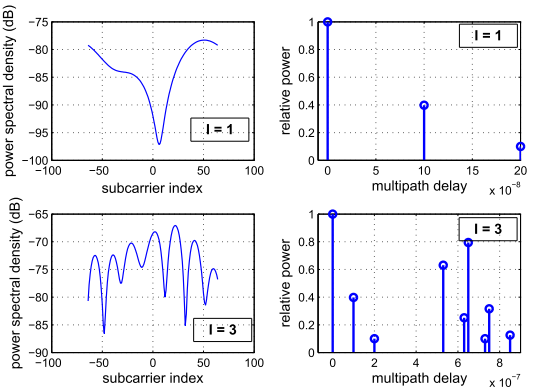

FIGURE 7. The PDP and PSD of the cooperative channel (with $I = 3$) compared to that of the PTP channel. The PSD is measured over a 10 MHz channel with 128-point FFT.

1) LARGE DYNAMIC RANGE

Channel simulations have been carried out to characterize the dynamic range of the PSD of the cooperative channel. Results are depicted in Figure 8 where the cumulative density function (CDF) of the PSD dynamic range is plotted for two cases, $I = 1$ and $I = 3$.

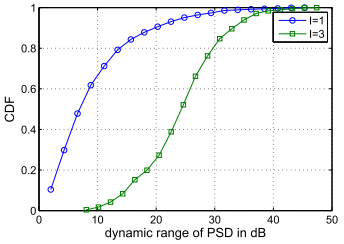

FIGURE 8. The CDF of the dynamic range of the PSD. The mean dynamic range was computed to be 10.1 dB in case of one transmitter (PTP case) and 25.3 dB in case of 3 cooperative transmitters.

The dynamic range of the channel's spectral response dictates the dynamic range of the receiver's FFT block. This is because OFDM receivers typically employ the

frequency-domain equalizers (FDE) to address the frequency selectivity of the channel. The FFT block must be able to cope with larger channel dynamic ranges. Otherwise, it will cause severe degradations in the FDE performance due to clipping and consequently it will adversely affect the overall receiver performance. In conclusion, the fixed-point design of the FFT block must accommodate the dynamic range requirements of cooperative transmission particularly in terms of memory resources allocated.

2) HIGH FREQUENCY SELECTIVITY

Indeed, best design practice calls for inserting pilots within the PHY frame. These pilots can be used to track phase and amplitude drifts of the channel coefficients. Pilot tones carry training symbols that are known a priori by the receiver in order to update the channel estimates. OFDM systems typically employ a comb-type pilot subcarrier arrangement whereby pilots are inserted regularly in the frequency domain [56].

Linear interpolation is mostly used to estimate channel coefficients at subcarriers between pilots. However, the frequency domain response of the cooperative channel is quite likely not to be linear between pilots. This is further illustrated in Figure 9. Accordingly, it is paramount to revert to non-linear interpolation. In the implementation presented in this paper, a 3-point quadratic interpolation is carried out in accordance with [57].

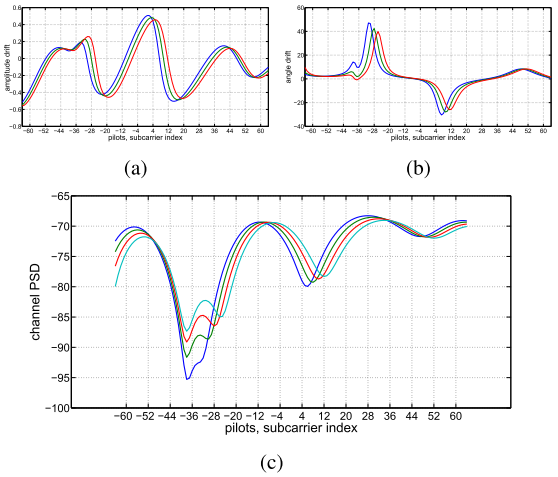

FIGURE 9. Frequency-domain response of the cooperative channel measured at pilot tones over consecutive OFDM symbols. The subcarrier indices shown in the plots correspond to the pilots. There are 8 pilots allocated within the 128-point FFT. (a) Amplitude drift. (b) Phase drift. (c) Power spectral density.

Lastly, it is worthy of noting that a modern robust forward error correction (FEC) scheme is poised to address many of the challenges associated with cooperative transmission. Low-density parity-check (LDPC) codes are great candidates for this purpose [50]. The same argument applies to the use of Turbo decoders. However, it is also important to note that the remedies outlined in this section are far less demanding in terms of onboard resource utilization compared to LDPC or Turbo codes. In one instance of implementation on field programmable gate array (FPGA) platform, the inclusion of a Turbo decoder increase resource utilization by nearly 40% compared to less than 10% for the suite of DDE, AGC update, and quadratic interpolation.

VI. FULLY AUTONOMOUS COOPERATIVE ROUTING

A. MOTIVATION

Route stability is defined as the probability that an end-to-end path connecting source to destination is still available after a certain duration from being established [58]. Indeed, ACR has been shown to offer better route stability compared to path-oriented MANET routing schemes under realistic mobility models [20]. In other words, ACR-based MANETs are substantially more tolerant to topological changes. Nevertheless, barrage regions still need to be maintained and regularly updated.

A barrage region must be initially created then regularly updated for each source-destination pair. In a convergecast mode (which is typical in mission-critical applications), this mandates the execution of a round-trip end-to-end handshake between each node in the network and the network sink. For a given node $\mathcal{U}$, the handshake process between $\mathcal{U}$ and the sink is essentially designed so that all other nodes can measure how many hops away from $\mathcal{U}$ they are [17]. This is then used to carve the barrage region from $\mathcal{U}$ to the sink. Denoting the hop-count from $\mathcal{U}$ to another node $\mathcal{V}$ with $\mathcal{C}(\mathcal{U}\mathcal{V})$, then a simple rule is to have nodes with $\mathcal{C}(\mathcal{U}\mathcal{V}) > \mathcal{Q}(\mathcal{U})$ suppress the transmission of $\mathcal{U}$'s packets [18].

While traffic in convergecast networks is predominantly upstream (traffic towards the sink), there is the need to cater for downstream traffic encompassing control and configuration messages. It is inaccurate however to consider that the barrage region in the upstream direction is good enough to represent that in the reverse direction, i.e. downstream. Reciprocity on weighted graphs (such as wireless networks) is a highly contentious issue [59]. As such, routes are generally non-reciprocal and consequently a barrage region has to be separately created for each direction of the traffic.

There are surely multiple approaches to manage the barrage region update process. It is important to note that the network can handle only one handshake process at a time. This is true since messages emanate from or terminate at a single node. Therefore, it is quite challenging to handle more than one update process at a time due to interference constraints. In other words, the network sink is required to orchestrate the barrage region update process. Assuming the sink has prior knowledge of all mobile nodes in the network, then one feasible approach consists of three phases:

1) A broadcast message from the sink soliciting a response from node $\mathcal{U}$. Intermediate nodes relaying the response message increment a designated hop-count field in the packet as it traverses the network towards $\mathcal{U}$.

2) A response message which is broadcast from node $\mathcal{U}$ back to the sink. Any intermediate node relaying the response message performs two tasks:
   a) Increments a designated hop-count field in the packet as it traverses the network towards the sink.
   b) Takes a decision whether it lies within or outside the downstream barrage region of $\mathcal{U}$.
3) To shape the upstream barrage region of $\mathcal{U}$, the sink has to rebroadcast another message containing the hop-count $Q(\mathcal{U})$ measured on the previous message. As this message traverses the network, each intermediate relay node decides whether it belongs within or beyond the upstream barrage region.

The process above is then sequentially repeated across the whole node population. Putting things into perspective, as the number of nodes N gets larger, the barrage region update process starts to have a tangibly significant overhead. This issue is discussed next.

In mission-critical operations, it is reasonable to mandate that all of the nodes complete the barrage creation/update process. Otherwise, nodes which are left out (for one reason or another) will resort to broadcasting, i.e. flooding, all of their frames. Undoubtedly, this causes substantial interference and unnecessarily overgrazes the network's spatial and temporal resources. As such, the barrage region creation/update process should target a 100% reachability. Reachability is a metric that measures the percentage of nodes which can be covered, i.e. are reachable, after performing $\mathcal{X}$ broadcast rounds [60]. Reachability is denoted by a positive monotonic function $R(\mathcal{X}) \leq 1$, where $\mathcal{X} = 0 \ldots \mathcal{X}_{max}$, $R(\mathcal{X}_{max}) = 1$, and $R(0) = 0$.

The barrage region handshake process has to be effectively executed with each node as many times as needed to reach that node. This actually contributes to increasing the duration of the barrage creation/update process. Subsequently, the effective number of nodes can be essentially defined as the number of times the handshake process is executed until barrage regions for all nodes have been established. Taking into consideration the fact that the handshake process consists of three broadcast phases, then the effective number of nodes is therefore given by:

$$N^{'} = N \left(\sum_{\mathcal{X}=1}^{\mathcal{X}_{max}} \mathcal{X} \left[R(\mathcal{X}) - R(\mathcal{X}-1) \right] \right)^{3}. \tag{27}$$

Another major factor to be considered relates to the fact that the hop-count is not a deterministic parameter but rather a discrete random variable. This is a fact of crucial importance since the hop-count from the source to the sink as well as to the intermediate nodes is the sole parameter used in defining the barrage region [18]. The number of hops measured from the traffic source $\mathcal{U}$ to an intermediate relay node $\mathcal{V}$ at round $\mathcal{X}$ is denoted by $\mathcal{C}_{\mathcal{X}}(\mathcal{UV})$. As a matter of fact, (17) can be used to derive the PMF of $\mathcal{C}(\mathcal{U})$ by substituting Q with $\mathcal{C}_{\mathcal{X}}(\mathcal{UV})$ and making D equal to the distance between the the $\mathcal{U}$ and $\mathcal{V}$.

Denoting the average hop-count by $\overline{\mathcal{C}}(\mathcal{UV})$, it can be demonstrated numerically, that the probability $\mathbb{P}[\mathcal{C}_{\mathcal{X}}(\mathcal{UV}) \neq \overline{\mathcal{C}}(\mathcal{UV}]$ has an appreciable value. An immediate conclusion can be drawn: the 3-way handshake process must be carried out more than once for each node, i.e. $S_R \geq 2$ times, in order to come up with an acceptable estimate of $\mathcal{C}(\mathcal{UV})$. Analysis of S_R and its relation to the confidence intervals of $\mathcal{C}(\mathcal{UV})$ is actually left off as follow up work to this paper.

Based on all of the above, the total time required to finish the barrage region creation/update process is given by:

$$T_U = 3 Q_{max} N^{'} T_h S_R, \tag{28}$$

where Q_{max} is the maximum number of hops required for the broadcast message to reach all nodes in the network. It is insightful at this point to put things into perspective using a numerical example. In [20] (Figure 4), it was shown that path availability probability drops below 95% after approximately 25 - 50 seconds.[3] Tactical and mission-critical MANETs can typically have as many 100 nodes [18]. Nodes are spread out such that up to 10 hops may be need for a broadcast message to cover the network [20]. The hop duration can be assumed to be in the range of $T_h = 500\mu$s which includes a very short packet transmission time, processing time and radio turn-around time. The effective number of nodes is highly influenced by $R(1)$ which is typically in the range of 95% [60]. Taking $R(\mathcal{X}) = [0.950, 0.990, 0.999, 1.000]$, then $N^{'} = 119$. Assuming $S_R = 2$, then (28) yields a whopping $T_U = 3.57$ seconds! This is at 14-28% contribution to the protocol overhead.

The barrage region creation/update overhead should also account for cases of network entry, i.e. new nodes joining the network. Join events will cut off the live network operation for a non-negligible period of time. So based on all of the above, there is sufficient rationale and motivation to fortify ACR with *full* autonomy, the subject of which is discussed in the next section.

B. FULL AUTONOMY ENABLED BY GEO-ROUTING

What would it take for a node to locally decide whether it should forward a given source's packet or not? What if a node is equipped with the capability to qualify whether its participation in the forwarding process is beneficiary to the packet's progress towards the sink? The availability of such a capability unleashes fully autonomous cooperative routing.

Knowledge of position relative to the sink is sufficient to meet that goal. During network initialization phase, the source sends a broadcast packet informing all other nodes of its position. Each node is also required to acquire its position relative to the sink. This can be done by means of an onboard global positioning system (GPS) module. Contrary to the classical perception, low-power GPS modules have

[3]The choice of a value for the path availability metric is indeed relative and subject to the underlying application. In mission-critical applications, robustness and high reliability are often stressed as key performance indicators by end-users. Thus, selecting 95% as a benchmark mainly stems from feedback the authors accumulated through interactions with end-users.

been commercially available for quite some time. As a matter of fact, power consumption by the GPS module is far less significant than other key components in wireless communications systems. For instance, the analog front-end is far more power-hungry than the GPS module as illustrated in Figure 10. Furthermore, the GPS module can be deeply duty-cycled to further save power.

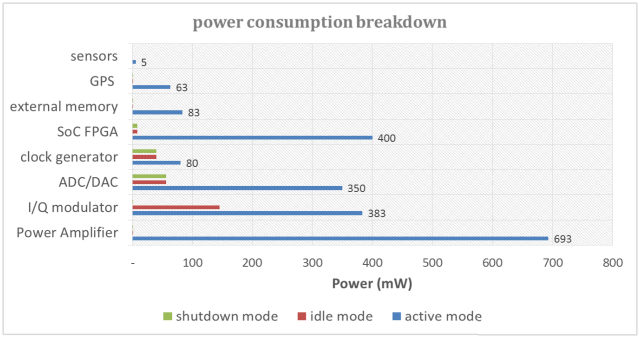

FIGURE 10. Various candidates for each component in the system have been surveyed with low power consumption as a prime objective. The survey quickly revealed that the analog front-end components (i.e. I/Q, PA, ADC/DAC) are the most power-hungry. Duty-cycling these components whenever possible is not only a good practice but a necessity. The power budget of the GPS module can be considered as insignificant.

The availability of position information allows the coupling of geo-routing and autonomous cooperative transmission. The result is full autonomy. This has been already eluded to in the illustration offered by Figure 2 in Section III. Full-length GPS positions are not really needed. Instead, each node needs to compute its relative position vector (distance and azimuth) with the origin being the sink. Furthermore, the system design has to cater for the very likely situation of weakening or complete black out of the GPS signal.

Fortunately, the time scale of node mobility is quite relaxed: loosing the GPS signal for a few seconds is likely to induce only intangible changes in the network topology. So it is more of an opportunistic approach which is advocated herewith where the position vector is updated whenever the GPS signal is accessible. Nonetheless, to account for those cases where a subset of nodes may suffer from prolonged GPS signal loss, a cooperative localization method is presented later in this section.

From a practical point of view, the challenge concerns the means by which cooperative transmitters can convey their position information to receivers (i.e. nodes who are potential the next-hop forwarders). An inherently related challenge is for this means to concurrently support the self-localization capability. The solution addressing both requirements is presented in the next subsection.

C. RANDOM ACCESS

To facilitate the communication of position information by transmitters, random access resources are allocated within the PHY frame as shown in Figure 11. The random access (RA) area consists of two distinct parts. The first one contains a

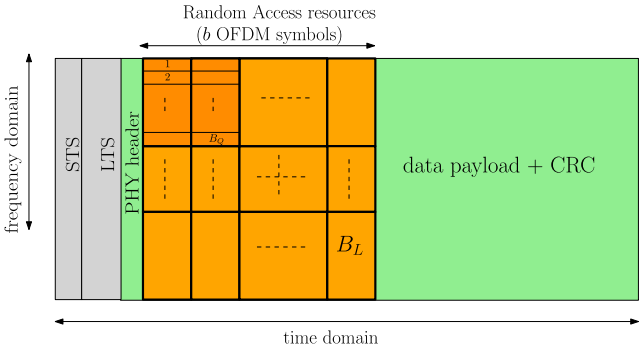

FIGURE 11. A random access (RA) area is inserted into the OFDM frame to support two capabilities: 1) allow cooperative transmitters to indicate the progress they offer towards the sink, and 2) encode their position information that can be used by receiver so as to perform a TDOA-based self-localization.

total of B_Q tones which are allocated for progress quantization purposes. The second part is consists of B_L resource blocks distributed over b OFDM symbols and are allocated explicitly for localization purposes. The design and processing considerations of the localization part of the RA area is discussed in the next subsection.

Before a cooperative transmitter sends a frame, it quantizes the progress it offers with respect towards the sink. There are B_Q quantization levels such that resolution is D/B_Q, where D is the distance between the source and the sink. Each step is allocated exactly one tone in the random access area shown in Figure 11. The relay needs to indicate the quantized progress it offers by simply energizing the corresponding tone whose index is equal to its progress level. Simple on-off keying (OOK) binary modulation is used to modulate the respective tone. At the receiver side, the B_Q tones will be routed from the output of the FFT stage towards the OOK demodulator as shown in Figure 12. Progress levels of the respective transmitters are extracted and fed to a routing decision module.

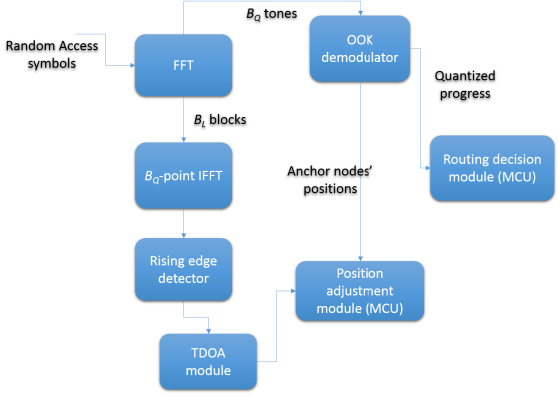

FIGURE 12. A block diagram illustrating the processing of the quantization tones and localization resource blocks, both part of the random access area illustrated in Figure 11.

Again, it is worthwhile to put things into perspective from a practical point of view. Nodes can be assumed to be

distributed over a finite 2D disc with diameter D_{max} according to a binomial point process (BPP) [61]. However, in a geo-routing context, the progress along the line connecting source to destination is what really matters. As such, the 2D BPP distribution can be projected or more precisely reduced to a 1D distribution. Consequently, the average distance to the ith nearest neighbor along the 1D progress dimension is given by $\frac{1}{2}ID_{max}/(N+1)$ [61]. The progress quantization level must be made sufficiently small to accommodate node displacement patterns. One viable design criterion is to have the quantization step D_{max}/B_Q larger than the distance to the Ith nearest cooperative transmitter along the progress line. In other words, it is to have

$$B_Q \geq 2(N+1)/I. \tag{29}$$

For $N = 100$ and $I = 3$ nodes, then $B_Q \geq 68$ tones which can be easily allocated within the stretch of one or two OFDM symbols.

D. LOCALIZATION

It has already been shown by [20] that it takes 25 - 50 seconds before the end-to-end path starts to become obsolete under realistic mobility models. A corollary to this is that nodes can afford to lose their GPS signals for an equivalently long duration. Nonetheless, there might be situations where some nodes may suffer from GPS signal blackouts for even longer durations. Mission-critical systems have to incorporate higher levels of resilience and robustness by definition and therefore need to account for such corner cases.

Nodes can capitalize on the presence of the random access area to carry out a triangulation procedure. Those nodes which enjoy clear GPS signals can transmit their position information on regular basis so that others without GPS access localize themselves. As shown in Figure 11, the random access area incorporates B_L resource blocks just for that purpose.

The method proposed for self-localization is to compute time difference of arrival (TDOA). Therefore, localization resource blocks need to cater two pieces of information: position information of the transmitters and propagation delay differences. The first one is straightforward and entails each anchor node encoding its position information into one of the localization blocks. A block is selected randomly by an anchor node and therefore collisions may occur. This is further discussed towards the end of this subsection. Within this context, anchor nodes simply represent that subset of transmitter nodes which still enjoy clear access to the GPS signal.

On the other hand, extraction of TDOA information exploits the fact that each uniquely selected resource block contains a signal with a unique time signature. This is further illustrated in Figure 13. The time reference at the receiver is influenced by the first energy arrival in the preamble portion of the frame. The B_L time waveforms must be reconstructed in order to detect the offset of each one from the zero time reference. As such, the B_L blocks are fed sequentially back to a B_Q-point IFFT module as depicted in Figure 12. The TDOA can then be measured.

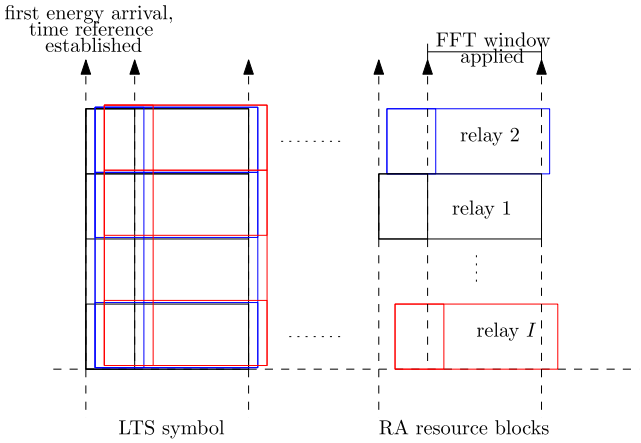

FIGURE 13. The localization random access resource blocks are offset from each other in time. This is due to the fact that each block is modulated by a different transmitter (obviously as long as it happens to be selected by one transmitter).

Inherent to any random access methodology, collisions may occur. Therefore, a sufficient number of resource blocks B_L should be allocated. It has been shown in [21] that when I nodes randomly access B_L random access resource blocks, the probability of at least $z \leq B_L$ uniquely selected blocks can be evaluated recursively using:

$$p_z = p_{z-1}\left(\frac{B-z}{B-z+1}\right)^{I-z}, \tag{30}$$

where $p_o = 1$. For triangulation purposes, at least three nodes are required. Subsequently, the success probability of self-localization for given received frame is given by:

$$p_{st} = \prod_{z=1}^{3}\left(\frac{B_L-z}{B_L-z+1}\right)^{I-z}, B_L \geq 3. \tag{31}$$

The number of frames until the triangulation function succeeds is denoted by F. Had I been constant, the mean F would have been represented by a geometric random variable whose mean is $\mathbb{E}[F] = 1/p_{st}$. Nonetheless, I is also randomly distributed and understanding its statistical behavior is nothing but trivial. This is true especially since the value of I depends on a multitude of factors including packet forwarding statistics and GPS signal loss patterns.

Having said that, I is expected to grow whenever the receiver is closer to the network sink and/or the GPS signal is less likely to be blocked. If I tends to be large, $\mathbb{E}[F]$ will also be, i.e. it will take a few frames before a node with lost GPS signal can triangulate itself. Fortunately however, when I tends to be large, this also implies that the expected number of nodes with lost GPS signal is small.

In any case, one can obtain a practical flavor of $\mathbb{E}[F]$ by noting that it is upper bounded by $1/p_{st}$ (evaluated at $\mathbb{E}[I]$). This is true by means of Jensen's inequality since it can be

directly shown using (31) that $\mathbb{E}[F]$ is strictly concave in terms of I. The value of $\mathbb{E}[F]$ has been computed for a range of $\mathbb{E}[I]$ and results are reported in Table 2. The table clearly shows that with only $B_L = 5$ blocks, there is ample time for nodes to adjust their positions. For the worst case scenario of $\mathbb{E}[I] = 7$, and assuming 1-ms frames, it takes no more than 82 ms to update the position.

TABLE 2. Average number of frames required until triangulation succeeds. A total of $B_L = 5$ resource blocks are assumed to be allocated in the random access area.

$\mathbb{E}[I]$	Situation	$\mathbb{E}[F]$
3	node closer to the network perimeter and/or heavy GPS signal blockage	2.08
5	node in the middle of the network and/or mild GPS signal loss	13.02
7	node close to the network sink and/or low likelihood of GPS signal loss	81.38

E. PRACTICAL IMPLEMENTATION CONSIDERATIONS

At the receiver, the preamble portion of the OFDM frame consists of identical replicas arriving asynchronously from I nodes. As shown in Figure 13, the receiver aligns its time reference to the first energy arrival of the first OFDM symbol. The receiver locks to the first energy arrival of the LTS symbol, which happens to be that of the 2nd relay in this example. The picture is fundamentally different in the RA portion where each non-empty block contains a unique signal (assuming no collisions).

RA signals are generally expected to be non-aligned in time, as illustrated in Figure 13. Time misalignments of the RA blocks obviously occur due to the differences in propagations delays between the relays towards the receiver in concern. Hence, for some RA blocks the FFT processing window at the receiver will not be aligned in time to the actual start of the RA signal within that block.

The effect of time offsets in OFDM systems was studied in [62]. Here, the time offset is ''towards'' the guard interval, i.e. the FFT window is partially applied on the guard interval. It was shown in [62] that such an offset only introduces a phase error. For this reason, OOK was chosen as a modulation scheme for convenience since it is indifferent to phase rotations. Reverting to OOK for the RA entails nearly negligble increase in the FPGA resource utilization footprint. On the other hand, the use of OOK modulation is surely associated with a 3 dB SNR penalty compared to using binary phase shift keying (BPSK) for example. Nevertheless, there is an inherent power boost on RA blocks. This is because all of the transmit RF power is focused on the RA block of choice at each transmitter. This indeed helps compensate for the SNR penalty.

On the other hand, it has already been mentioned that the reconstruction of the localization waveforms is done sequentially. Such an approach is affordable since the time budget of the localization process is not quite constrained. In other words, it is acceptable for a node to take a few seconds to adjust its position information. Therefore, dedicated FPGA resources need not be allocated for localization. Instead, available resources can be exploited opportunistically. In fact, the relaxed time constraint allows to solve the hyperbolic equations associated with the triangulation function in a more powerful microcontroller processing unit (MCU), as suggested in Figure 12.

Finally, it is worthwhile to have a peak under the hood on how the RA can be practically implemented. For a 128-point FFT, B_Q is set at 128 tones divided equally and contiguously over two consecutive symbols. Setting and $b = 6$, and allocating 64 tones per localization block yields $B_L = 5$ blocks. For 100-symbol OFDM frames, this an overhead contribution of just 6%. If the localization capability is switched off (i.e. in case of low likelihood of GPS signal loss), the overhead goes down to less than 1%. This is tangibly better than the 14 - 28% incurred by ACR predecessors.

According to (29), 64 quantization tones are good enough to serve $N = 95$ nodes with an average of $I = 3$ cooperative transmitters. At the other end, each OOK-modulated localization block has 128 tones or equivalently bits. With a rate $\frac{1}{2}$ FEC, this leaves 64 bits out of which 4 can be used for parity. It can be straightforwardly shown that the remaining 60 bits are sufficient to represent the GPS position offset of a node from the sink.

On the other hand, the localization resolution is actually function of the sampling rate and the number of subcarriers in each localization block. At 40 Msps, and noting that the number of samples per block is half of that of the whole OFDM symbol, then the resolution that can be achieved is 30 meters. A high-performance ADC capable of higher sampling rates is indeed slightly more expensive but - if needed - can be used to achieve better resolution.

VII. EXPERIMENTAL RESULTS

A. DEVELOPMENT PLATFORM

Off-the-shelf OFDM-based transceivers (e.g. standard-based IEEE 802.11a/g or IEEE 802.16d/e) cannot be used for experimenting with cooperative transmission schemes [50]. This is due to the fact that cooperation invokes substantial changes to the PHY and lower MAC layers. Moreover, the challenges described in Section V mandate a more robust PHY design. Hence, it was decided to build the ACR/FACR protocol stack completely from scratch so as to have a sufficient level of flexibility and control over the design process.

To that end, a compact stand-alone software-defined radio (SDR) platform was selected (Figure 14). A complete 128-point OFDM PHY was developed entirely for this project. The PHY supports channel bandwidths from 1 - 20 MHz with ADC sampling rates up to 40 Msps. The cyclic prefix consists of 32 samples such that the total number of samples per symbol is 160. The chosen SDR is home for a 40-KLE Altera Cyclone IV FPGA, an ARM9 micro-controller architecture, and a reconfigurable radio frequency (RF) chip from Lime Microsystems. An RF

FIGURE 14. An SDR platform from Nuand was used to build the fully autonomous cooperative routing scheme. The platform houses a 40-KLE Altera Cyclone IV FPGA, a Cypress micro-controller unit (MCU), and a reconfigurable RF chipset from Lime Microsystems. An RF amplifier from Texas Instruments was also annexed to the platform. The OFDM PHY was built on the FPGA, while the rest of the protocol stack runs on the MCU.

amplifier from Texas Instruments was also annexed to the platform. The OFDM PHY was built on the FPGA, while the rest of the protocol stack runs on the MCU.

The original plan was to install the SDR platforms on highly mobile stations to test PHY performance. However, it was shown in Section V-B that the CCFO effect produces a channel that is much more dynamic and time-varying than that produced by doppler spread, even at high speeds. A corollary to this is that empirical results collected from the field under CCFO with *stationary* nodes are sufficient to ensure the implementation will successfully handle mobility. The key parameters concerning the underlying PHY design is reported in Table 3.

TABLE 3. Key OFDM PHY design parameters.

channel bandwidth	1 - 20 MHz
frequency spectrum	0.3 - 3.8 GHz
maximum RF transmit power	10 dBm
antenna gain	3 dBi
FFT size	128 points
maximum sampling rate	40 Msps
preamble length (STS+LTS)	768 samples
number of pilots	8
turn-around time	180μs
useful symbol length	128 samples
cyclic prefix length	32 samples

B. EQUALIZER PERFORMANCE

The performance of the DDE implementation was investigated under a controlled setup. A dedicated BladeRF board was configured to feed 3 other boards with two common

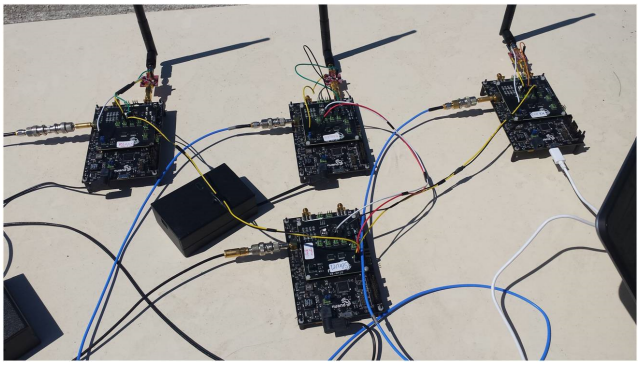

FIGURE 15. Common clock and trigger signals are fed into the boards. The controlled test setup is used to measure the performance of the decision-directed equalization method.

signals: clock and trigger, as shown in Figure 15. The latter is used to instruct the 3 relays to commence the transmission of a frame that is pre-stored on the FPGA. The CFO is invoked locally at each transmitting node via a command line interface (CLI) utility. Similarly, each node my be configured to introduce a fixed delay after the rising edge of the trigger signal. This can be used to produce the desired delay spread for the composite channel. In other words, it helps control the propagation delays $T_1^{'}, \ldots, T_I^{'}$ shown in Figure 4.

In this test, the three transmitters were placed 12 meters from the receiver. The CFO values for the transmitters were set at -100, 500, and 1000 Hz. A 16 quadrature amplitude modulation (16-QAM) modulation scheme with FEC rate of 1/2 was used. As expected, DDE is quite a viable tool to equalize highly time-varying channels. Run over a large number of iterations, the average frame error rate (FER) plunged from 81% down to less than 5% when the DDE module was activated at the receiver. The error vector magnitude (EVM) of the baseband inphase/quadrature (I/Q) stream was measured on randomly selected subset of frames in MATLAB (Figure 16). The average EVM ascended from as low as -6 dB to 14 dB. Neglecting transmitter I/Q imperfections, the EVM is known to be tightly related to the receiver SNR. As such, the DDE module can be said to offer a gain of nearly 20 dB while introducing less than 5% in the overall footprint of the PHY code. These results are summarized in Table 4.

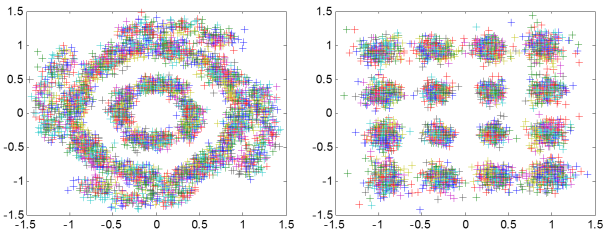

FIGURE 16. DDE performance investigated for the case of concurrent transmission from three nodes with CFO1 = 1000 Hz, CFO2 = 0 Hz, CFO3 = $-$100Hz. Here, the received I/Q symbols is plotted.

TABLE 4. DDE performance results.

	traditional equalizer	decision-driven equalizer (DDE)
FER	81%	5%
EVM	-6 dB	14 dB
highest modulation	BPSK	16 QAM

C. ARRAY GAIN

The goal of this test case was to measure the array gain as well as the maximum reach gain that can be obtained by means of autonomous cooperative transmission. The same setup presented in the previous subsection was used. To obtain the maximum reach gain, the CFO was forced to zero on all three transmitters. The three transmitters were always kept equidistant from the receiver. The test was carried out in an open space parking lot surrounded by light vegetation. All nodes were placed one meter above ground level. Results of this test are reported in Table 5. Each result corresponds to an average value taken over an ensemble of of 10,000 frames.

TABLE 5. Results from the array gain test.

	SNR (dB)	RSSI (dBm)	FER	reach (meters)
Tx_1 only	16.1	-88.2	2.9%	70
	11.2	-93.1	50.8%	115
Tx_2 only	16.5	-87.5	0.8 %	65
	11.8	-94.1	76.2 %	115
Tx_3 only	16.4	-88.0	1.1%	65
	12.4	-93.5	47.0%	115
all three	16.3	-86.7	2.0%	115

The first stage of this stage was to measure the communication range for each individual transmitter. The communication range here was defined as the maximum reach such that an average FER target of $\leq$ 3% is maintained. The receiver was gradually moved away in steps of 5 meters. As reported in Table 5, the communication range was around 65 - 70 meters. The slight discrepancy in results are due the different multipath channels since transmitters are not co-located. Another factor is the approximate nature of any method for computing the SNR on the preamble signal.

Next, the communication range for the case of three cooperative transmitters was measured by gradually moving the receiver away in steps of 5 meters. The maximum range was measured to be 115 meters, i.e. the reach gain was 50 meters or equivalently 77%. Indeed, the reach gain highly depends on the propagation characteristics which in return relates to the environment where the test is performed.

Now in order to characterize the array gain, each transmitter was placed 115 meters away from the receiver and the SNR was measured. The array gain is computed here as the difference between the SNR obtained under coopertive transmission and the average of individual SNR values. It is clear from Table 5 that autonomous cooperative transmission is able to offer nearly 4.5 dB of array gain. This result is quite interesting since it is very close to the theoretical maximum array gain with 3 transmitters, i.e. $10 \log 3 = 4.77$ dB.

VIII. CONCLUSIONS

By nature, mission-critical applications are delay intolerant. Furthermore, there is a growing trend of bandwidth-hungry use cases within the realm of mission-critical operations. Off-the-shelf standardized wireless technologies have been shown to fall short in scenarios deemed essential in mission-critical contexts. As such, mobile ad hoc networking (MANET) has resurfaced again as a viable candidate. Having said that, classical path-oriented MANET routing techniques are notoriously known to accumulate substantial protocol overhead as the network grows in scale. Subsequently, it has been shown that autonomous cooperative routing (ACR) is well positioned to meet the goals and aspirations of mission-critical operations.

To that end, the implementation of ACR on hardware platforms entails a few practical challenges which have not been quite addressed in literature. The foremost challenge concerns the receiver's capability in handling the aggressive nature of the cooperative wireless channel. The cooperative channel is highly time-varying therefore causing channel estimates to become obsolete pretty quickly. A robust channel equalizer based on the use of decision-drive estimation (DDE) was presented to remedy this issue. On the other hand, the cooperative channel has been shown to feature a high level of selectivity in the spectral domain which was handled by means of optimized pilot processing.

The paper also presented some obvious shortcoming of contemporary implementations of ACR, specifically the need for regular topological updates. As such a fully astomous version was presented and analyzed. Moreover, practical implementation considerations have been also highlighted offering some evidence of the advents of full autonomy.

Finally, the paper presented an experimental setup that was developed specifically for this project. A protocol stack was built from scratch for that purpose. Field experiments were carried out and were able to validate some of the performance enhancement propositions outlined in the previous sections of the paper.

ACKNOWLEDGEMENT

The authors would like to acknowledge Karim Abed-Meraim and Mohamed Tlich for their invaluable advice and technical support throughout this project. Karim suggested the use of decision-driven estimation and equalization method for addressing the highly time-varying nature of the cooperative channel. He has also provided guidance on how to implement it from an algorithmic point of view. On the other hand, Mohamed was quite instrumental in the experimentation aspects pertaining to this project. He provided a few instrumental PHY core modules necessary for building the test bed developed for the project.

REFERENCES

[1] S. Ghafoor, P. D. Sutton, C. J. Sreenan, and K. N. Brown, "Cognitive radio for disaster response networks: Survey, potential, and challenges," *IEEE Wireless Commun.*, vol. 21, no. 5, pp. 70–80, Oct. 2014.

[2] I. F. Akyildiz, T. Melodia, and K. R. Chowdhury, "A survey on wireless multimedia sensor networks," *Comput. Netw.*, vol. 51, no. 4, pp. 921–960, Mar. 2007.

[3] Z.-J. Zhang, C.-F. Lai, and H.-C. Chao, "A green data transmission mechanism for wireless multimedia sensor networks using information fusion," *IEEE Wireless Commun.*, vol. 21, no. 4, pp. 14–19, Aug. 2014.

[4] L. Yang, S. H. Yang, and L. Plotnick, "How the Internet of things technology enhances emergency response operations," *Technol. Forecast. Social Change*, vol. 80, no. 9, pp. 1854–1867, Mar. 2013.

[5] P. R. Chai, "Wearable devices and biosensing: Future frontiers," *J. Med. Toxicol.*, vol. 12, no. 4, pp. 332–334, Jun. 2016.

[6] A. Panayides, Z. C. Antoniou, Y. Mylonas, M. S. Pattichis, A. Pitsillides, and C. S. Pattichis, "High-resolution, low-delay, and error-resilient medical ultrasound video communication using H.264/AVC over mobile WiMAX networks," *IEEE J. Biomed. Health Informat.*, vol. 17, no. 3, pp. 619–628, May 2013.

[7] F. Bergstrand and J. Landgren, "Using live video for information sharing in emergency response work," *Int. J. Emergency Manage.*, vol. 6, nos. 3–4, pp. 295–301, 2009.

[8] A. Blair, T. Brown, K. M. Chugg, T. R. Halford, and M. Johnson, "Barrage relay networks for cooperative transport in tactical manets," in *Proc. IEEE Military Commun. Conf. MILCOM*, Nov. 2008, pp. 1–7.

[9] X. Lin, J. Andrews, A. Ghosh, and R. Ratasuk, "An overview of 3GPP device-to-device proximity services," *IEEE Commun. Mag.*, vol. 52, no. 4, pp. 40–48, Apr. 2014.

[10] A. Bader, H. Ghazzai, A. Kadri, and M.-S. Alouini, "Front-end intelligence for large-scale application-oriented Internet-of-things," *IEEE Access*, vol. 4, pp. 3257–3272, Jun. 2016.

[11] L. Carlà, R. Fantacci, F. Gei, D. Marabissi, and L. Micciullo, "LTE enhancements for public safety and security communications to support group multimedia communications," *IEEE Netw.*, vol. 30, no. 1, pp. 80–85, Jan./Feb. 2016.

[12] M. Gharbieh, H. ElSawy, A. Bader, and M.-S. Alouini, "Tractable stochastic geometry model for IoT access in LTE networks," in *Proc. IEEE Globecom*, Washington, USA, Dec. 2016.

[13] W. Kiess and M. Mauve, "A survey on real-world implementations of mobile ad-hoc networks," *Ad Hoc Netw.*, vol. 5, no. 3, pp. 324–339, 2007.

[14] B. Bellalta, "IEEE 802.11ax: High-efficiency WLANs," *IEEE Wireless Commun.*, vol. 23, no. 1, pp. 38–46, Feb. 2016.

[15] A. Abouzeid and N. Bisnik, "Geographic protocol information and capacity deficit in mobile wireless ad hoc networks," *IEEE Trans. Inf. Theory*, vol. 57, no. 8, pp. 5133–5150, Aug. 2011.

[16] *Request for Information, Novel Methods for Information Sharing in Large Scale Mobile Ad-Hoc Networks, Defense Advanced Research Projects Agency (DARPA)*, document DARPA-SN-13-35, Apr. 2013.

[17] T. R. Halford, K. M. Chugg, and A. Polydoros, "Barrage relay networks: System & protocol design," in *Proc. IEEE 21st Int. Symp. Pers. Indoor Mobile Radio Commun.*, Sep. 2010, pp. 1133–1138.

[18] T. R. Halford and K. M. Chugg, "Barrage relay networks," in *Proc. Inf. Theory Appl. Workshop (ITA)*, Jan. 2010, pp. 1–8.

[19] U. G. Acer, S. Kalyanaraman, and A. A. Abouzeid, "Weak state routing for large-scale dynamic networks," *IEEE/ACM Trans. Netw.*, vol. 18, no. 5, pp. 1450–1463, Oct. 2010.

[20] T. R. Halford and K. M. Chugg, "The stability of multihop transport with autonomous cooperation," in *Proc. Military Commun. Conf. (MILCOM)*, Nov. 2011, pp. 1023–1028.

[21] A. Bader, K. Abed-Meraim, and M.-S. Alouini, "An efficient multi-carrier position-based packet forwarding protocol for wireless sensor networks," *IEEE Trans. Wireless Commun.*, vol. 11, no. 1, pp. 305–315, Jan. 2012.

[22] L. V. Thanayankizil, A. Kailas, and M. A. Ingram, "Opportunistic large array concentric routing algorithm (OLACRA) for upstream routing in wireless sensor networks," *Ad Hoc Netw.*, vol. 9, no. 7, pp. 1140–1153, 2011.

[23] C.-K. Ke, Y.-L. Chen, Y.-C. Chang, and Y.-L. Zeng, "Opportunistic large array concentric routing algorithms with relay nodes for wireless sensor networks," *Comput. Electr. Eng.*, vol. 56, pp. 350–365, Nov. 2016.

[24] F. Bergstrand and J. Landgren, "Visual reporting in time-critical work: Exploring video use in emergency response," in *Proc. 13rd Int. Conf. Human Comput. Int. Mobile Devices Services*, 2011, pp. 415–424.

[25] D. S. Nunes, P. Zhang, and J. S. Silva, "A survey on human-in-the-loop applications towards an Internet of all," *IEEE Commun. Surv. Tuts.*, vol. 17, no. 2, pp. 944–965, 2nd Quart. 2015.

[26] R. Felts, M. Leh, and T. McElvaney, "Public safety analytics R&D roadmap," U.S. Dept. Commerce, Nat. Inst. Standards Technol., Gaithersburg, MD, USA, Tech. Note 1917, Apr. 2016.

[27] J. Fink, A. Ribeiro, and V. Kumar, "Robust control of mobility and communications in autonomous robot teams," *IEEE Access*, vol. 1, pp. 290–309, 2013.

[28] I. Bayezit and B. Fidan, "Distributed cohesive motion control of flight vehicle formations," *IEEE Trans. Ind. Electron.*, vol. 60, no. 12, pp. 5763–5772, Dec. 2013.

[29] J. A. J. Berni, P. J. Zarco-Tejada, L. Suarez, and E. Fereres, "Thermal and narrowband multispectral remote sensing for vegetation monitoring from an unmanned aerial vehicle," *IEEE Trans. Geosci. Remote Sens.*, vol. 47, no. 3, pp. 722–738, Mar. 2009.

[30] S. Siebert and J. Teizer, "Mobile 3D mapping for surveying earthwork projects using an unmanned aerial vehicle (UAV) system.," *Autom. Construct.*, vol. 41, pp. 1–14, Feb. 2014.

[31] T. R. Halford, T. A. Courtade, and K. A. Turck, "The user capacity of barrage relay networks," in *Proc. Military Commun. Conf. (MILCOM)*, Oct. 2012, pp. 1–6.

[32] X. Xiang, X. Wang, and Z. Zhou, "Self-adaptive on-demand geographic routing for mobile ad hoc networks," *IEEE Trans. Mobile Comput.*, vol. 11, no. 9, pp. 1572–1586, Sep. 2012.

[33] *Intelligent Transport Systems (ITS); Vehicular Communications; Geonetworking; Part 4: Geographical Addressing and Forwarding for Point-to-Point and Point-to-Multipoint Communications; Sub—Part 1: Media-Independent Functionality, v1.2.0*, document ETSI TS 102 636-4-1 V1.1.1, Oct. 2013.

[34] J. A. Sanchez, P. M. Ruiz, and R. Marin-Perez, "Beacon-less geographic routing made practical: Challenges, design guidelines, and protocols," *IEEE Commmun. Mag.*, vol. 47, no. 8, pp. 85–91, Aug. 2009.

[35] A. Scaglione, D. L. Goeckel, and J. N. Laneman, "Cooperative communications in mobile ad hoc networks," *IEEE Signal Process. Mag.*, vol. 23, no. 5, pp. 18–29, Sep. 2006.

[36] B. Sirkeci-Mergen and A. Scaglione, "Randomized space-time coding for distributed cooperative communication," *IEEE Trans. Signal Process.*, vol. 55, no. 10, pp. 5003–5017, Oct. 2007.

[37] B. Sirkeci-Mergen and A. Scaglione, "Randomized space-time coding for distributed cooperative communication," *IEEE Trans. Signal Process.*, vol. 55, no. 10, pp. 5003–5017, Oct. 2007.

[38] M. Sharp, A. Scaglione, and B. Sirkeci-Mergen, "Randomized cooperation in asynchronous dispersive links," *IEEE Trans. Commun.*, vol. 57, no. 1, pp. 64–68, Jan. 2009.

[39] Y. Li, Z. Zhang, C. Wang, W. Zhao, and H.-H. Chen, "Blind cooperative communications for multihop ad hoc wireless networks," *IEEE Trans. Veh. Technol.*, vol. 62, no. 7, pp. 3110–3122, Sep. 2013.

[40] T. R. Halford and K. M. Chugg, "Barrage relay networks," in *Proc. Inf. Theory Appl. Workshop (ITA)*, Jan. 2010, pp. 1–8.

[41] R. H. Brian and G. Hwang, "Barrage relay networks for unmanned ground systems," in *Proc. Military Commun. Conf. (MILCOM)*, Oct. 2010, pp. 1274–1280.

[42] D. K. Lee and K. M. Chugg, "A pragmatic approach to cooperative communication," in *Proc. IEEE Military Commun. Conf. (MILCOM)*, Oct. 2006, pp. 1–7.

[43] A. Bader and M.-S. Alouini, "Localized power control for multihop large-scale Internet of things," *IEEE Internet Things J.*, vol. 3, no. 4, pp. 503–510, Aug. 2016.

[44] M. Zorzi and R. R. Rao, "Geographic random forwarding (GeRaF) for ad hoc and sensor networks: Multihop performance," *IEEE Trans. Mobile Comput.*, vol. 2, no. 4, pp. 337–348, Oct. 2003.

[45] P. Gupta and P. R. Kumar, "The capacity of wireless networks," *IEEE Trans. Inf. Theory*, vol. 46, no. 2, pp. 388–404, Mar. 2000.

[46] N. Bisnik and A. A. Abouzeid, "Queuing network models for delay analysis of multihop wireless ad hoc networks," *Ad Hoc Netw.*, vol. 7, no. 1, pp. 79–97, Jan. 2009.

[47] N. Bisnik and A. A. Abouzeid, "Queuing delay and achievable throughput in random access wireless ad hoc networks," in *Proc. 3rd Annu. IEEE Commun. Soc. Sensor Ad Hoc Commun. Netw.*, vol. 3. Sep. 2006, pp. 874–880.

[48] H. Wu, Y. Peng, K. Long, S. Cheng, and J. Ma, "Performance of reliable transport protocol over IEEE 802.11 wireless lan: Analysis and enhancement," in *Proc. 21st Annu. Joint Conf. IEEE Comput. Commun. Soc. (INFOCOM)*, vol. 2. 2002, pp. 599–607.

[49] A. Bader, K. Abed-Meraim, and M. S. Alouini, "Reduction of buffering requirements: Another advantage of cooperative transmission," *IEEE Sensors J.*, vol. 15, no. 4, pp. 2017–2018, Apr. 2015.
[50] H. Qiu, K. Wang, K. Psounis, G. Caire, and K. M. Chugg, "High-rate wifi broadcasting in crowded scenarios via lightweight coordination of multiple access points," in *Proc. 17th ACM Int. Symp. Mobile Ad Hoc Netw. Comput. (MobiHoc)*, Jul. 2016, pp. 301–310.
[51] T. S. Rappaport, *Wireless Communications: Principles and Practice*, 2nd ed. Englewood Cliffs, NJ, USA: Prentice-Hall, 2001.
[52] H. Schulze and C. Lueders, *Theory and Applications of OFDM and CDMA: Wideband Wireless Communications*, 1st ed. New York, NY, USA: Wiley, 2005.
[53] B. Zhao and M. C. Valenti, "Practical relay networks: A generalization of hybrid-ARQ," *IEEE J. Sel. Areas Commun.*, vol. 23, no. 1, pp. 7–18, Jan. 2005.
[54] T. Rouphael, *Wireless Receiver Architectures and Design* (Antennas, RF, Synthesizers, Mixed Signal, and Digital Signal Processing), 1st ed. New York, NY, USA: Elsevier, 2014.
[55] J. Ran, R. Grunheid, H. Rohling, E. Bolinth, and R. Kern, "Decision-directed channel estimation method for OFDM systems with high velocities," in *Proc. 57th IEEE Semiannu. Veh. Technol. Conf.*, vol. 4, Apr. 2003, pp. 2358–2361.
[56] M.-H. Hsieh and C.-H. Wei, "Channel estimation for OFDM systems based on comb-type pilot arrangement in frequency selective fading channels," *IEEE Trans. Consum. Electron.*, vol. 44, no. 1, pp. 217–225, Feb. 1998.
[57] S. Coleri, M. Ergen, A. Puri, and A. Bahai, "Channel estimation techniques based on pilot arrangement in OFDM systems," *IEEE Trans. Broadcast.*, vol. 48, no. 3, pp. 223–229, Sep. 2002.
[58] A. B. McDonald and T. F. Znati, "A mobility-based framework for adaptive clustering in wireless ad hoc networks," *IEEE J. Sel. Areas Commun.*, vol. 17, no. 8, pp. 1466–1487, Aug. 1999.
[59] T. Squartini, F. Picciolo, F. Ruzzenenti, and D. Garlaschelli, "Reciprocity of weighted networks," *Sci. Rep.*, vol. 3, p. 2729, Sep. 2013.
[60] M. Eriksson and A. Mahmud, "Dynamic single frequency networks in wireless multihop networks—Energy aware routing algorithms with performance analysis," in *Proc. IEEE 10th Int. Conf. Comput. Inf. Technol.*, Bradford, U.K., May 2010, pp. 400–406.
[61] S. Srinivasa and M. Haenggi, "Distance distributions in finite uniformly random networks: Theory and applications," *IEEE Trans. Veh. Technol.*, vol. 59, no. 2, pp. 940–949, Feb. 2010.
[62] C. R. N. Athaudage, "BER sensitivity of OFDM systems to time synchronization error," in *Proc. 8th Int. Conf. Commun. Syst. (ICCS)*, vol. 1. Singapore, Nov. 2002, pp. 42–46.

AHMED BADER (M'10–SM'13) received the B.S. degree in electrical engineering from The University of Jordan in 2003, the M.S. degree in electrical engineering from The Ohio State University in 2006, and the Ph.D. degree in electrical engineering from Télécom ParisTech, France, in 2013. He has over 10 years of experience in the wireless industry and has held positions with Emerson and Siemens. Since 2013, he has been with the King Abdullah University of Science and Technology, Saudi Arabia, where he is spearheading multiple applied research projects that led into several patent-pending technologies. He is also a Co-Founder of Insyab Wireless, a Dubai-based company designing real-time connectivity solutions for unmanned systems. His research interests are mainly in the domain of large-scale wireless networks.

MOHAMED-SLIM ALOUINI (S'94–M'98–SM'03–F'09) was born in Tunis, Tunisia. He received the Ph.D. degree in electrical engineering from the California Institute of Technology, Pasadena, CA, USA, in 1998. He served as a Faculty Member with the University of Minnesota, Minneapolis, MN, USA, and then with the Texas A&M University at Qatar, Education City, Doha, Qatar. He was with the King Abdullah University of Science and Technology, Thuwal, Saudi Arabia, as a Professor of Electrical Engineering in 2009. His current research interests include the modeling, design, and the performance analysis of wireless communication systems.